Available online at www.sciencedirect.com
ScienceDirect
Journal of Sound and Vibration 312 (2008) 644–671
JOURNAL OF SOUND AND VIBRATION
www.elsevier.com/locate/jsvi

Waveguide finite elements for curved structures

Svante Finnveden*, Martin Fraggstedt

The Marcus Wallenberg Laboratory for Sound and Vibration Research (MWL), Royal Institute of Technology, 100 44 Stockholm, Sweden

Received 8 March 2007; received in revised form 4 August 2007; accepted 5 November 2007
Available online 21 December 2007

Abstract

A waveguide finite element formulation for the analysis of curved structures is introduced. The formulation is valid for structures that along one axis have constant properties. It is based on a modified Hamilton's principle valid for general linear viscoelastic motion, which is derived here. Using this principle, material properties such as losses may be distributed in the system and may vary with frequency. Element formulations for isoparametric solid elements and deep shell elements are presented for curved waveguides as well as for straight waveguides. In earlier works, the curved elements have successfully been used to model a passenger car tyre. Here a simple validation example and convergence study is presented, which considers a finite length circular cylinder and all four elements presented are used, in turn, to model this structure. Calculated results compare favourably to those in the literature.

1. Introduction

In a "low-frequency" analysis of vibration in a built-up structure, the eigenfrequencies and the corresponding eigenmodes help the understanding of how and why the structure behaves as it does. These eigensolutions are also useful in calculations of forced response by modal superposition procedures. However, as frequency increases there are more and more modes with increasingly complex forms and the relative information content in each of them decreases. The level and distribution of damping also becomes increasingly important. For such "high-frequency" motion it is therefore beneficial to change view point and describe the motion in terms of damped waves, in particular so if the structure is "long" in one direction. If, moreover, it has constant geometrical and material properties along this direction, wave solutions can be found with a versatile and numerically efficient method—the waveguide finite element method (FEM).

The first applications of the waveguide FEM were Lagasse's [1] work on the eigenmodes of topographic waveguides of arbitrary cross section and Aalami's analysis of wave propagation and edge resonances in rods of arbitrary cross section [2]. Both appeared in 1973. Later applications describe wave motion in straight structures of increasing complexity, see, e.g., the recent references [3–8] where literature reviews are found.

When the waveguide FEM describes the free harmonic motion of a structure, it results in a set of coupled ordinary differential equations (ODE). The solutions to these equations are wave functions that describe the

*Corresponding author.
E-mail address: svantef@kth.se (S. Finnveden).

0022-460X/$ - see front matter © 2007 Elsevier Ltd. All rights reserved.
doi:10.1016/j.jsv.2007.11.020

wave form and the propagation and decay along the structure as functions of frequency. These solutions are useful for diagnostic purposes, e.g., in Ref. [3] the size and location of blocking masses was decided based on a waveguide finite elements analysis (FEA) of a wind tunnel and in Ref. [9] a similar analysis of a railway car base frame helped devising a high-frequency and a low-frequency statistical energy analysis (SEA) model. Also, the effect of damping treatments is directly inferred from waveguide FEA results [7,8].

The results from a waveguide FEA can be used in, at least, three different ways to synthesise the forced response of structures.

(a) For an infinite waveguide, a spatial Fourier transform of the ODEs gives algebraic equations that are easily solved. The response is then given by an inverse Fourier transform, made by a residue calculus in which the poles are defined by the free wave solutions discussed above [10].
(b) The damped wave solutions can be used as basis functions in a new, spectral, FE formulation for a finite length waveguide. Such a spectral superelement is formulated in Ref. [11] where it is shown that it could be put into an assembly and be combined with other spectral elements and with conventional finite elements, thus providing high computational efficiency in some cases.
(c) Certain "convenient" boundary conditions are fulfilled by a wave solution together with a companion wave travelling in the opposite direction. For such boundary conditions, the eigenmodes of a finite length structure are directly identified by a two-dimensional waveguide FEA, which has a much lower computational cost than a conventional three-dimensional FEA. Once the eigenmodes are identified, a modal analysis gives the forced response of the structure. In Ref. [10] the "convenient" boundary condition for a straight waveguide was the shear diaphragm condition, in which all motion within the cross section is blocked while all motion along the waveguide is free.

This article, and Refs. [12,13], models structures with another "convenient" boundary condition namely that for a circular structure the response is a periodic function of the angular coordinate. This requires that new waveguide FEMs for curved structures are developed, which is this article's first major contribution. It appears the only previous formulations for such elements are the conical thin-shell element and the fluid element presented by Nilsson [5]. Refs. [23,24], however, describe special elements for curved waveguides in the form of radius pipe bends. For this special geometry, Hayashi et al. derive new elements that efficiently describes propagating waves. Demma et al. [24] also calculates propagating waves using the so-called axi-symmetric finite elements, see, e.g., Refs. [14,15]. Such elements are widely used both for dynamic and static problems, and are found in commercial software. As noted by Nilsson, when modelling a full circular structures with curved waveguide FEM, the equations of motion equal those arrived with using axi-symmetric elements. The presented waveguide finite elements can be used for this while they are more resourceful. They can be used for studies of damped wave motion in curved structures and they can form the basis of spectral superelements of substructures with an arbitrary arc length, including near field components at the element ends.

Finite elements are often based on weak formulations, e.g., in Ref. [14] it is based on the principle of virtual work and in Ref. [15] it is based on Garlerkin's method. There are, however, some advantages with a variational formulation and therefore the elements presented here are based on a modified Hamilton's principle, valid for viscoelastic material. This principle has been used by the first author in previous publications, e.g., in Refs. [4,16]. In Ref. [16] it was validated simply by noting that for the cylinder, the equations of motion derived from the principle, are identical to those derived from dynamic equilibrium [18]. It was motivated by reference to Morse and Feshbach [19, Chapter 3], Gladwell [20] and Morse and Ingard [21, Section 6.2], where the idea of using an adjoint negatively damped system can be found. Ref. [4] demonstrated the principle for an Euler beam, considering a simple relaxation function, while the present work derives it for linear motion of general viscoelastic material. To the best of the authors' knowledge, this derivation is presented here for the first time, which is the article's other major contribution.

The short-term goal of the present work is to model car tyre vibrations. The elements derived here are in Refs. [12,13], used in a waveguide FE model of a car tyre, where it is validated by a modal analysis in lower frequency range and by point and transfer mobility measurements up to 1 kHz. The agreement between

measurements and predictions is good. These measurements are also the basis for evaluating the viscoelastic losses of the investigated tyre, which are not known a priori.

The measurements and predictions in Refs. [12,13] confirm the usefulness of the elements derived in the present article. Therefore only a simple validation example is considered here, namely a circular cylinder. The advantages with this example is that all elements presented can be used to model it and that exact results, based on three-dimensional theory, are available in the Ref. [18].

The outline of the article is as follows. Section 2 presents a derivation of a modified Hamilton's principle for linear viscoelastic motion upon which a general formulation of waveguide finite elements follows. Sections 3 and 4 then derive the waveguide finite elements for curved solid elements and curved deep shell elements. Section 5 derives the corresponding elements for straight waveguides. Section 6 uses, in turn, all four elements to calculate eigenfrequencies for a circular cylinder and Section 7 concludes the article.

2. A variational principle for linear viscoelastic motion

This section presents a derivation of a modified Hamilton's principle for linear viscoelastic motion upon which a general formulation of waveguide finite elements follows. This formulation is in the following sections used for deriving solid and deep-shell elements for curved and straight waveguides. The derivation of the variational principle for viscoelastic material follows quite closely the corresponding derivation for elastic material in Fung and Tong [17, Chapter 10 and 11], which is recommended.

2.1. Displacements and strains

The first step in a variational formulation is to explicitly identify the generalised coordinates that are varied. Here, an FE displacement formulation is sought and finite elements for isotropic solids and deep shells are considered. The solid's motion is then given by a three-dimensional displacement field, while the shell's motion is given by the displacements at its midsurface plus the rotations about two orthogonal axes on the surface. These displacements are the generalised coordinates and are collected in a vector: $\mathbf{u}$, which is a function of time (t) and location (x).

In linear motion, the strain is given by a linear combination of the displacement and its spatial derivatives. The strain–displacement relations are given by

$$\boldsymbol{\varepsilon} = \mathscr{E}(\mathbf{u}), \tag{1}$$

where $\mathscr{E}$ is a linear differential operator and the entries to the engineering strain vector $\boldsymbol{\varepsilon}$ are the strain components that contributes to the strain energy, ordered in a convenient fashion. Examples are given in Sections 3–5.

2.2. Constitutive equations, strain energy and Hamilton's principle

The constitutive equation relates the strains to the stresses. For a linear elastic material, the engineering stress vector, $\boldsymbol{\sigma}$, is given by

$$\boldsymbol{\sigma} = \mathbf{D}\boldsymbol{\varepsilon}, \tag{2}$$

where the rigidity matrix $\mathbf{D}$ is symmetric and positive semi-definite. Fung and Tong define the strain energy function, W, such that [17, Chapter 10]

$$\boldsymbol{\sigma}_j = \partial W/\partial \boldsymbol{\varepsilon}_j. \tag{3}$$

It follows that the strain energy function is a potential, giving the stresses as functions of the strains. For a linear elastic material it is

$$W = \tfrac{1}{2}\boldsymbol{\varepsilon}^{\mathrm{T}}\mathbf{D}\boldsymbol{\varepsilon}, \tag{4}$$

where $^{\mathrm{T}}$ indicates the transpose of a vector or a matrix.

If the external load on the structure is independent of its motion, as is commonly the case, the potential energy of the loading, A, exists and is a linear function of the displacements:

$$A = -\int_V \mathbf{f}^{\mathrm{T}}\mathbf{u}\,\mathrm{d}V - \int_{S_\sigma} \mathbf{n}^{\mathrm{T}}\mathbf{T}\mathbf{u}\,\mathrm{d}S, \tag{5}$$

where V is the structure's domain, $\mathbf{f}$ is the body forces acting on it and S_σ is the surface, with outward normal $\mathbf{n}$, where the external traction $\mathbf{T}$ is prescribed. On the rest of the boundary there are either homogenous natural boundary conditions or prescribed displacements. The latter, essential, boundary conditions must be imposed directly on the displacements, since they cannot vary on this part of the boundary.

Upon this basis, Fung and Tong demonstrate, for static problems, the principle of the minimum potential energy [17, Chapter 10.7]

$$\delta(U + A) = 0, \tag{6}$$

where δ denotes the first variation and U is the total strain energy of the structure,

$$U = \int_V W\,\mathrm{d}V. \tag{7}$$

Similarly, for dynamic problems Hamilton's principle is demonstrated [17, Chapter 11.1]

$$\delta \int_{t_1}^{t_2} (U - K + A)\,\mathrm{d}t = 0, \tag{8}$$

where

$$K = \frac{1}{2}\int_V \rho \left(\frac{\partial \mathbf{u}}{\partial t}\right)^{\mathrm{T}} \left(\frac{\partial \mathbf{u}}{\partial t}\right) \mathrm{d}V \tag{9}$$

is the kinetic energy of the structure and ρ is the density.

2.3. Viscoelastic material

The stress in a viscoelastic material depends on the strain and also on its history. For a general linear viscoelastic material, the stress is given by a convolution integral as follows [17, Chapter 15]:

$$\boldsymbol{\sigma}(x,t) = \mathscr{D}(\boldsymbol{\varepsilon}) \equiv \int_{-\infty}^{t} \mathbf{G}(x, t-\tau)\frac{\partial \boldsymbol{\varepsilon}}{\partial \tau}(x,\tau)\,\mathrm{d}\tau, \tag{10}$$

where $\mathscr{D}$ is a linear operator and the entries to the matrix $\mathbf{G}$ are linear combinations of the material's relaxation functions. Examples of material models that can be written on the form of Eq. (10) include generalised Maxwell and Kelvin models [17], fractional derivative models [22] and the Augmented Hooke's law [25,26].

Hamilton's principle does not apply for viscoelastic material. Mathematically speaking, the reason for this is that the operator $\mathscr{D}$ is not self-adjoint and because of this, the strain energy functional is not a potential and the variational machinery cannot be used. The operator $\mathscr{D}^A$ that is adjoint to $\mathscr{D}$ is defined by the following relation:

$$\int \mathbf{u}^{\mathrm{T}}\mathscr{D}(\mathbf{v})\,\mathrm{d}t = \int \mathbf{v}^{\mathrm{T}}\mathscr{D}^A(\mathbf{u})\,\mathrm{d}t. \tag{11}$$

In Appendix A, it is demonstrated that, if the Fourier transforms of $\mathbf{u}$ and $\mathbf{v}$ exist, $\mathscr{D}^A$ is given by

$$\mathscr{D}^A(\mathbf{u}) \equiv \int_t^{\infty} -\mathbf{G}(x, \tau - t)\frac{\partial \mathbf{u}}{\partial \tau}(x,\tau)\,\mathrm{d}\tau. \tag{12}$$

Now, we will have a variational principle for viscoelastic material and therefore need a potential. One option is then the following bi-linear form:

$$\hat{W} = \tfrac{1}{4}(\boldsymbol{\varepsilon}^{A\mathrm{T}}\mathscr{D}(\boldsymbol{\varepsilon}) + \boldsymbol{\varepsilon}^{\mathrm{T}}\mathscr{D}^A(\boldsymbol{\varepsilon}^A)) \tag{13}$$

which, obviously, is self-adjoint. $\boldsymbol{\varepsilon}^A$ is the strain in the adjoint system. This adjoint system is excited by the same forces as the system of interest and is in all aspects identical to this system except for that the material does not obey the constitutive relation given by Eq. (10) but

$$\boldsymbol{\sigma}^A = \mathscr{D}^A(\boldsymbol{\varepsilon}^A). \tag{14}$$

The strain potential function $\hat{W}$ has the property that

$$\delta \int \hat{W}\,\mathrm{d}t = \frac{1}{2}\int \boldsymbol{\sigma}^{\mathrm{T}}\delta\boldsymbol{\varepsilon}^A\,\mathrm{d}t + \frac{1}{2}\int \boldsymbol{\sigma}^{A\mathrm{T}}\delta\boldsymbol{\varepsilon}\,\mathrm{d}t \tag{15}$$

and may therefore be used in a variational principle. This modified Hamilton's principle is given by bi-linear forms, similar to the one in Eq. (13). Thus, instead of the work made by external forces in Eq. (5), we use the load potential

$$\hat{A} = -\frac{1}{2}\int_V (\mathbf{f}^{\mathrm{T}}\mathbf{u} + \mathbf{f}^{\mathrm{T}}\mathbf{u}^A)\,\mathrm{d}V - \frac{1}{2}\int_{S_\sigma} \mathbf{n}^{\mathrm{T}}(\mathbf{T}\mathbf{u} + \mathbf{T}\mathbf{u}^A)\,\mathrm{d}S \tag{16}$$

and instead of the kinetic energy in Eq. (9), we use the kinetic potential

$$\hat{K} = \frac{1}{2}\int_V \rho\left(\frac{\partial \mathbf{u}^A}{\partial t}\right)^{\mathrm{T}}\left(\frac{\partial \mathbf{u}}{\partial t}\right)\mathrm{d}V. \tag{17}$$

Also, we define the total strain potential

$$\hat{U} = \int_V \hat{W}\,\mathrm{d}V. \tag{18}$$

The modified Hamilton's principle states that

$$\delta \int (\hat{U} - \hat{K} + \hat{A})\,\mathrm{d}t = 0. \tag{19}$$

It is demonstrated in Appendix B that it is true provided that the displacements obey the equation of dynamic equilibrium and the boundary conditions. The full variational machinery can therefore be used. In particular, Eq. (19) is a sound basis for approximate methods, such as the finite element method.

2.4. Harmonic motion

If the responses are harmonic on the form of

$$\mathbf{u}(t) = \mathrm{Re}(\tilde{\mathbf{u}}\mathrm{e}^{-\mathrm{i}\omega t}) = \tfrac{1}{2}(\tilde{\mathbf{u}}\mathrm{e}^{-\mathrm{i}\omega t} + \tilde{\mathbf{u}}^*\mathrm{e}^{\mathrm{i}\omega t}),$$

$$\mathbf{u}^A(t) = \mathrm{Re}(\tilde{\mathbf{u}}^A\mathrm{e}^{-\mathrm{i}\omega t}) = \tfrac{1}{2}(\tilde{\mathbf{u}}^A\mathrm{e}^{-\mathrm{i}\omega t} + \tilde{\mathbf{u}}^a\mathrm{e}^{\mathrm{i}\omega t}) \tag{20}$$

it is possible to simplify principle (19). Above, $\tilde{\mathbf{u}}$ denotes the complex amplitude of the displacements, $\tilde{\mathbf{u}}^*$ denotes the complex conjugate of $\tilde{\mathbf{u}}$ and upper index "a" is introduced for "A^*," so that $\tilde{\mathbf{u}}^a = (\tilde{\mathbf{u}}^A)^*$.

The time average of the kinetic potential is given by

$$\langle\hat{K}\rangle = \frac{1}{T}\int_V \int_{-T/2}^{T/2} \frac{1}{2}\rho\left(\frac{\partial \mathbf{u}^A}{\partial t}\right)^{\mathrm{T}}\left(\frac{\partial \mathbf{u}}{\partial t}\right)\mathrm{d}t\,\mathrm{d}V = \frac{1}{8}(\bar{K} + \bar{K}^*), \tag{21}$$

where T is the period time, an integer multiple of the period time or a time very much longer than this, $\bar{K}$ is given by

$$\bar{K} = \int_V \rho\omega^2\tilde{\mathbf{u}}^{a\mathrm{T}}\tilde{\mathbf{u}}\,\mathrm{d}V. \tag{22}$$

Similar calculations give that

$$\langle\hat{A}\rangle = \tfrac{1}{8}(\bar{A} + \bar{A}^*),$$

$$\bar{A} = -\int_V (\tilde{\mathbf{f}}^{\mathrm{H}}\tilde{\mathbf{u}} + \tilde{\mathbf{f}}^{\mathrm{T}}\tilde{\mathbf{u}}^a)\,\mathrm{d}V - \int_{S_\sigma} \mathbf{n}^{\mathrm{T}}(\tilde{\mathbf{T}}^*\tilde{\mathbf{u}} + \tilde{\mathbf{T}}\tilde{\mathbf{u}}^a)\,\mathrm{d}S, \tag{23}$$

where $^{\mathrm{H}}$ indicates the complex conjugate and transpose of a matrix, and

$$\langle \hat{U} \rangle = \tfrac{1}{8}(\bar{U} + \bar{U}^*), \tag{24}$$

$$\begin{aligned}
\bar{U} &= \frac{1}{2}\int_V \left(\frac{1}{T}\int_{-T/2}^{T/2}\left(\tilde{\boldsymbol{\varepsilon}}^{a\mathrm{T}}\mathrm{e}^{\mathrm{i}\omega t}\int_{-\infty}^{t}\mathbf{G}(t-\tau)(-\mathrm{i}\omega\tilde{\boldsymbol{\varepsilon}}\mathrm{e}^{-\mathrm{i}\omega\tau})\,\mathrm{d}\tau\right)\mathrm{d}t\right)\mathrm{d}V \\
&\quad + \frac{1}{2}\int_V \left(\frac{1}{T}\int_{-T/2}^{T/2}\tilde{\boldsymbol{\varepsilon}}\mathrm{e}^{-\mathrm{i}\omega t}\left(\int_{t}^{\infty}-\mathbf{G}(\tau-t)(\mathrm{i}\omega\tilde{\boldsymbol{\varepsilon}}^{a\mathrm{T}}\mathrm{e}^{\mathrm{i}\omega\tau})\,\mathrm{d}\tau\right)\mathrm{d}t\right)\mathrm{d}V \\
&= \frac{1}{2}\int_V \tilde{\boldsymbol{\varepsilon}}^{a\mathrm{T}}\left(\frac{1}{T}\int_{-T/2}^{T/2}\mathrm{e}^{\mathrm{i}\omega t}\mathrm{e}^{-\mathrm{i}\omega t}\int_{-\infty}^{t}-\mathrm{i}\omega\mathbf{G}(t-\tau)\mathrm{e}^{-\mathrm{i}\omega(\tau-t)}\,\mathrm{d}\tau\right)\tilde{\boldsymbol{\varepsilon}}\,\mathrm{d}t\,\mathrm{d}V \\
&\quad + \frac{1}{2}\int_V \tilde{\boldsymbol{\varepsilon}}\left(\frac{1}{T}\int_{-T/2}^{T/2}\mathrm{e}^{-\mathrm{i}\omega t}\mathrm{e}^{\mathrm{i}\omega t}\int_{t}^{\infty}-\mathrm{i}\omega\mathbf{G}(\tau-t)\mathrm{e}^{\mathrm{i}\omega(\tau-t)}\,\mathrm{d}\tau\right)\tilde{\boldsymbol{\varepsilon}}^{a\mathrm{T}}\,\mathrm{d}t\,\mathrm{d}V \\
&= \int_V (\tilde{\varepsilon}^{a\mathrm{T}}\tilde{\mathbf{D}}\tilde{\boldsymbol{\varepsilon}})\,\mathrm{d}V,
\end{aligned} \tag{25}$$

where, using that the relaxation function is zero for negative arguments, the complex rigidity matrix $\tilde{\mathbf{D}}$ is given by

$$\tilde{\mathbf{D}} = \int_{-\infty}^{t}-\mathrm{i}\omega\mathbf{G}(t-\tau)\mathrm{e}^{-\mathrm{i}\omega(\tau-t)}\,\mathrm{d}\tau = \int_{-\infty}^{\infty}-\mathrm{i}\omega\mathbf{G}(\tau)\mathrm{e}^{\mathrm{i}\omega\tau}\,\mathrm{d}\tau \tag{26}$$

and is thus given by the Fourier transform of the relaxation function. The real part of the rigidity matrix $\tilde{\mathbf{D}}$ describes the material's elastic properties, while the imaginary part describes the damping.

The analysis above was made for one harmonic component. Similar expressions apply also if the harmonic decomposition is built upon a Fourier series expansion or a Fourier transform, since for linear systems the motion at different frequencies do not couple. The common factor $\frac{1}{8}$ in Eqs. (21), (23) and (24) may be dropped, since we are just looking for a linear relation between response and excitation. Also, it suffices to consider the first term on the right-hand sides of these equations, since the functional built by the second terms is just the complex conjugate of the functional built by the first terms and if the variation of one functional is zero so is the other. Upon this basis, the modified principle for harmonic response is

$$\delta L = \delta(\bar{U} - \bar{K} + \bar{A}) = 0, \tag{27}$$

where L is denoted the Lagrangian (out of habit).

The variational principle for viscoelastic motion in Eq. (19), and for harmonic motion in Eq. (27), is the most important theoretical result in this work. The most important practical results are the formulations, in Sections 3–5, of waveguide finite elements for the evaluation of the strain potential $\bar{U}$ and the kinetic potential $\bar{K}$. First, in the next sub section, the waveguide FE approach for solving Eq. (27) in the absence of excitation is reviewed.

2.5. Waveguide finite element formulation

In an FEA the displacements are approximated by polynomial shape functions, which are non-zero within one element only. The amplitude of the shape functions are given by the displacements at nodes. An appropriate choice of the shape functions ensure that the displacement fields are continuous between elements, so, they have "compact support" and the functionals in Eq. (27) can be evaluated for each of the elements in turn.

In a waveguide FEA the displacements dependence on the cross-sectional coordinates is approximated only. For curved structures, the displacements are in a cylindrical coordinate system thus given by

$$\begin{aligned}
\tilde{\mathbf{u}}(r,x,\phi) &= \mathbf{N}(r,x)\tilde{\mathbf{v}}(\phi), \\
\tilde{\mathbf{u}}^{\mathrm{a}}(r,x,\phi) &= \mathbf{N}(r,x)\tilde{\mathbf{v}}^a(\phi),
\end{aligned} \tag{28}$$

where r is the radial coordinate, x is the axial coordinate, the entries to the matrix $\mathbf{N}$ are two-dimensional FE shape functions and the entries of the vectors $\tilde{\mathbf{v}}$ and $\tilde{\mathbf{v}}^a$ are the "nodal" displacements, which are functions of the angular coordinate ϕ.

The strain–displacement relations (1) are written in a split operator form and the derivatives with respect to r and x are evaluated:

$$\tilde{\boldsymbol{\varepsilon}} = \mathscr{E}(\tilde{\mathbf{u}}) = \mathbf{E}_0(r,x)\tilde{\mathbf{v}}(\phi) + \mathbf{E}_1(r,x)\frac{\partial \tilde{\mathbf{v}}(\phi)}{\partial \phi}, \tag{29}$$

where the matrices $\mathbf{E}_0$ and $\mathbf{E}_1$ contain FE shape functions and derivatives of these, defined by the strain–displacement relations and the FE approximations (28).

Upon this basis, and in the absence of external forces, the Lagrangian is given by

$$\begin{aligned} L &= \sum_l \int_{V_l} (\tilde{\boldsymbol{\varepsilon}}^{a\mathrm{T}} \tilde{\mathbf{D}} \tilde{\boldsymbol{\varepsilon}} - \rho\omega^2 \tilde{\mathbf{u}}^{a\mathrm{T}} \tilde{\mathbf{u}})\, \mathrm{d}V \\ &= \sum_l \int_{V_l} \left(\sum_{n=0}^{1} \sum_{m=0}^{1} \left(\frac{\partial^n \tilde{\mathbf{v}}_l^{a\mathrm{T}}}{\partial \phi^n} \mathbf{E}_n^{\mathrm{T}} \tilde{\mathbf{D}} \mathbf{E}_m \frac{\partial^m \tilde{\mathbf{v}}_l}{\partial \phi^m} \right) - \tilde{\mathbf{v}}_l^{a\mathrm{T}} \mathbf{N}^{\mathrm{T}} \rho\omega^2 \mathbf{N} \tilde{\mathbf{v}}_l \right) \mathrm{d}V, \end{aligned} \tag{30}$$

where the summation is taken over the elements, V_l is the domain of element l and $\mathbf{v}_l$ is the subset of nodes connected to the element. The elements can be put into an assembly and thus model a great variety of structures. The assembled Lagrangian will be of the form of

$$L = \int \left(\sum_{n=0}^{1} \sum_{m=0}^{1} \left(\frac{\partial^n \tilde{\mathbf{v}}^{a\mathrm{T}}}{\partial \phi^n} \mathbf{A}_{nm} \frac{\partial^m \tilde{\mathbf{v}}}{\partial \phi^m} \right) - \omega^2 \tilde{\mathbf{v}}^{a\mathrm{T}} \mathbf{M} \tilde{\mathbf{v}} \right) \mathrm{d}\phi, \tag{31}$$

where $\mathbf{M}$ is a mass matrix and the matrices $\mathbf{A}_{nm}$ are generalised stiffness matrices. In the absence of external forces the Lagrangian in Eq. (31) is stationary for true motion. The corresponding Euler–Lagrange equations constitute a set of coupled ordinary differential equations

$$\mathbf{K}_2 \frac{\partial^2 \tilde{\mathbf{v}}}{\partial \phi^2} + \mathbf{K}_1 \frac{\partial \tilde{\mathbf{v}}}{\partial \phi} + \mathbf{K}_0 \tilde{\mathbf{v}} - \omega^2 \mathbf{M} \tilde{\mathbf{v}} = 0, \tag{32}$$

where

$$\mathbf{K}_2 = -\mathbf{A}_{11}, \quad \mathbf{K}_1 = \mathbf{A}_{01} - \mathbf{A}_{10}^{\mathrm{T}}, \quad \mathbf{K}_0 = \mathbf{A}_{00}. \tag{33}$$

The matrices in Eq. (32) have constant entries and therefore the solutions are exponential functions on the form of

$$\tilde{\mathbf{v}}(\phi) = \hat{\mathbf{v}} \mathrm{e}^{\mathrm{i}\kappa\phi}, \tag{34}$$

where $\hat{\mathbf{v}}$ denotes the wave amplitude.

If Eq. (34) is substituted into Eq. (32) a twin-parameter eigenvalue problem follows. Either a linear eigenvalue problem for a given wave order, κ, could be solved or a quadratic eigenvalue problem for a given frequency, ω. The solutions to any of these eigenvalue problems are of interest in their own right and can also be used to synthesise forced response as discussed in Section 1 and in Refs. [3,5,10–12].

The following sections consider the formulation of isotropic solid elements and deep shell elements for curved waveguides as well as for straight waveguides. Solutions to Eq. (32) as well as to the corresponding equation for straight waveguides are then considered in Section 6.

3. Isoparametric solid waveguide finite element

3.1. Geometry and coordinate transformation

Consider the nine node element in Fig. 1. It is formulated in a cylindrical coordinate system (x, r, ϕ), related to the Cartesian coordinates (X, Y, Z) as $X = x$, $Y = r\cos\phi$, $Z = r\sin\phi$. Fig. 1 describes the cross section at $\phi = 0$ where $r = Y$.

The geometry of the element and the displacements are interpolated with quadratic shape functions, which for ease of numerical manipulation are partitioned as $\mathbf{hB}_0$, where the row vector $\mathbf{h}$ contains polynomials and $\mathbf{B}_0$ is a projection matrix. These are given by

$$\mathbf{h}(\xi,\eta)=\begin{bmatrix}1 & \xi & \xi^2 & \eta & \eta\xi & \eta\xi^2 & \eta^2 & \eta^2\xi & \eta^2\xi^2\end{bmatrix}, \tag{35}$$

$$\mathbf{h}(\xi_n,\eta_n)\mathbf{B}_0=\mathbf{I}, \quad n=1,2,\ldots,9, \tag{36}$$

where $\mathbf{I}$ is an identity matrix and

$$(\xi_1,\eta_1)=(-1,-1), \quad (\xi_2,\eta_2)=(0,-1),\ldots,(\xi_9,\eta_9)=(0,0). \tag{37}$$

Thus, node number one is located in the lower left corner, the following nodes are numbered anticlockwise and finally, node number nine is within the element. With these shape functions, the global coordinates are given by the transformation

$$x=\mathbf{h}(\zeta,\eta)\mathbf{b}_x, \quad r=\mathbf{h}(\zeta,\eta)\mathbf{b}_r, \tag{38}$$

where the vectors $\mathbf{b}_x$ and $\mathbf{b}_r$ are given by

$$\mathbf{b}_x=\mathbf{B}_0\begin{bmatrix}X_1\\X_2\\\vdots\\X_9\end{bmatrix}, \quad \mathbf{b}_r=\mathbf{B}_0\begin{bmatrix}Y_1\\Y_2\\\vdots\\Y_9\end{bmatrix}, \tag{39}$$

(X_n, Y_n) is the location of node number n in Cartesian coordinates at $\phi=0$.

3.2. Displacements

The variables of response, the displacements u, v and w in the $x-$, $r-$ and ϕ-directions, respectively, are described by polynomial shape functions and variational parameters $\mathbf{v}$

$$\mathbf{u}(x,y,z)=\begin{bmatrix}u\\v\\w\end{bmatrix}=\begin{bmatrix}\mathbf{h}(\xi,\eta)\mathbf{B}_u\\\mathbf{h}(\xi,\eta)\mathbf{B}_v\\\mathbf{h}(\xi,\eta)\mathbf{B}_w\end{bmatrix}\mathbf{v}(\phi), \tag{40}$$

where the entries to $\mathbf{v}(\phi)$ are the nodal displacements; in fact, the displacements along a line. The 9×27 matrices $\mathbf{B}_u$, $\mathbf{B}_v$, $\mathbf{B}_w$ each have nine non-zero columns which are those of $\mathbf{B}_0$ ordered according to the definition of $\mathbf{v}$. Note, here and in what follows the tilde sign above the response variables and the rigidity matrix are ommited for breviety. Also note that the material parameters may be frequency dependant.

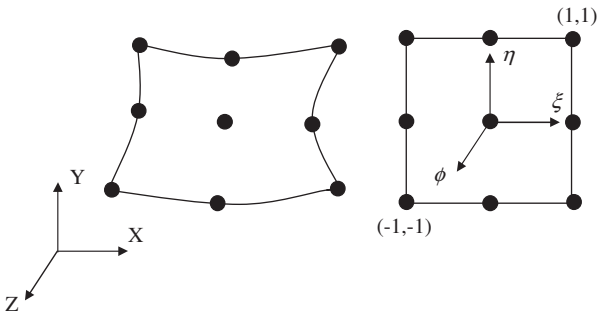

Fig. 1. Left, example of nine-node element. Right, parent element, for which the integration is made.

3.3. Strain displacement relations

In a cylindrical coordinate system, the engineering strain vector is given by

$$\boldsymbol{\varepsilon} = \begin{bmatrix} \varepsilon_x & \varepsilon_r & \varepsilon_\phi & \gamma_{xr} & \gamma_{x\phi} & \gamma_{r\phi} \end{bmatrix}^{\mathrm{T}}, \tag{41}$$

where

$$\begin{aligned} &\varepsilon_x = \frac{\partial u}{\partial x}, \quad \varepsilon_r = \frac{\partial v}{\partial r}, \quad \varepsilon_\phi = \frac{1}{r}\frac{\partial w}{\partial \phi} + \frac{v}{r}, \\ &\gamma_{xr} = \frac{\partial v}{\partial x} + \frac{\partial u}{\partial r}, \quad \gamma_{x\phi} = \frac{\partial w}{\partial x} + \frac{1}{r}\frac{\partial u}{\partial \phi}, \quad \gamma_{r\phi} = \frac{\partial w}{\partial r} - \frac{w}{r} + \frac{1}{r}\frac{\partial v}{\partial \phi}. \end{aligned} \tag{42}$$

Now, the displacements (40) are inserted into Eq. (41) and the strain vector is partitioned as in Eq. (29), where

$$\mathbf{E}_0 = \begin{bmatrix} \mathbf{h}_x\mathbf{B}_u \\ \mathbf{h}_r\mathbf{B}_v \\ \mathbf{h}\mathbf{B}_v/r \\ \mathbf{h}_x\mathbf{B}_v + \mathbf{h}_r\mathbf{B}_u \\ \mathbf{h}_x\mathbf{B}_w \\ \mathbf{h}_r\mathbf{B}_w - \mathbf{h}\mathbf{B}_w/r \end{bmatrix}, \quad \mathbf{E}_1 = \frac{1}{r}\begin{bmatrix} 0 \\ 0 \\ \mathbf{h}\mathbf{B}_w \\ 0 \\ \mathbf{h}\mathbf{B}_u \\ \mathbf{h}\mathbf{B}_v \end{bmatrix} \tag{43}$$

and

$$\begin{bmatrix} \mathbf{h}_x \\ \mathbf{h}_r \end{bmatrix} \equiv \begin{bmatrix} \dfrac{\partial \mathbf{h}}{\partial x} \\ \dfrac{\partial \mathbf{h}}{\partial r} \end{bmatrix} = \mathbf{J}^{-1}\begin{bmatrix} \dfrac{\partial \mathbf{h}}{\partial \xi} \\ \dfrac{\partial \mathbf{h}}{\partial \eta} \end{bmatrix}, \tag{44}$$

$$\mathbf{J} = \begin{bmatrix} \dfrac{\partial x}{\partial \xi} & \dfrac{\partial r}{\partial \xi} \\ \dfrac{\partial x}{\partial \eta} & \dfrac{\partial r}{\partial \eta} \end{bmatrix} = \begin{bmatrix} \dfrac{\partial \mathbf{h}}{\partial \xi}\mathbf{b}_x & \dfrac{\partial \mathbf{h}}{\partial \xi}\mathbf{b}_r \\ \dfrac{\partial \mathbf{h}}{\partial \eta}\mathbf{b}_x & \dfrac{\partial \mathbf{h}}{\partial \eta}\mathbf{b}_r \end{bmatrix}. \tag{45}$$

In Eq. (43), and in what follows, 0 denotes a matrix of zeros of appropriate dimensions.

3.4. The Lagrangian

In the absence of excitation the Lagrangian is given by Eq. (30). In which the rigidity matrix $\mathbf{D}$, for an isotropic material, is given by

$$\mathbf{D} = \begin{bmatrix} \mathbf{D}_{00} & 0 \\ 0 & \mathbf{D}_{11} \end{bmatrix}, \quad \mathbf{D}_{00} = \frac{E}{(1+\nu)(1-2\nu)}\begin{bmatrix} 1-\nu & \nu & \nu \\ \nu & 1-\nu & \nu \\ \nu & \nu & 1-\nu \end{bmatrix}, \quad \mathbf{D}_{11} = G\begin{bmatrix} 1 & 0 & 0 \\ 0 & 1 & 0 \\ 0 & 0 & 1 \end{bmatrix}, \tag{46}$$

where E is Young's modulus, ν is Poisson's ratio and the shear modulus $G = E/2(1+\nu)$. Losses are attributed if these elastic parameters are frequency dependent and complex.

In cylindrical coordinates and using the isoparametric element we have

$$\begin{aligned} L &= \int\int\int_{-1}^{1} (\boldsymbol{\varepsilon}^{a\mathrm{T}}\mathbf{D}\boldsymbol{\varepsilon} - \omega^2\mathbf{u}^{a\mathrm{T}}\rho\mathbf{u})r|\det(\mathbf{J})|\,\mathrm{d}\xi\,\mathrm{d}\eta\,\mathrm{d}\phi \\ &= \int\left(\sum_{n=0}^{1}\sum_{m=0}^{1}\frac{\partial^n\mathbf{v}^{a\mathrm{T}}}{\partial\phi^n}\mathbf{A}_{nm}\frac{\partial^m\mathbf{v}}{\partial\phi^m} - \omega^2\mathbf{v}^{a\mathrm{T}}\mathbf{M}\mathbf{v}\right)\mathrm{d}\phi, \end{aligned} \tag{47}$$

where

$$\mathbf{A}_{nm} = \int_{-1}^{1}\int_{-1}^{1} \mathbf{E}_n^{\mathrm{T}}\mathbf{D}\mathbf{E}_m r|\det(\mathbf{J})|\,\mathrm{d}\xi\,\mathrm{d}\eta, \tag{48}$$

$$\mathbf{M} = (\mathbf{B}_u^{\mathrm{T}}\mathbf{M}_0\mathbf{B}_u + \mathbf{B}_v^{\mathrm{T}}\mathbf{M}_0\mathbf{B}_v + \mathbf{B}_w^{\mathrm{T}}\mathbf{M}_0\mathbf{B}_w), \tag{49}$$

$$\mathbf{M}_0 = \int_{-1}^{1}\int_{-1}^{1} (\mathbf{h}^{\mathrm{T}}\rho\mathbf{h})r|\det(\mathbf{J})|\,\mathrm{d}\xi\,\mathrm{d}\eta. \tag{50}$$

The integrals in Eqs. (48) and (50) are evaluated with Gauss quadrature, easily applied for the square domain in Fig. 1, see, e.g., [14, Chapter 8].

4. Isoparametric doubly-curved deep-shell waveguide-FE

Consider the three-node shell section in Fig. 2. The geometry of the element and the displacements are interpolated with quadratic shape functions $\mathbf{N}(\xi) = \mathbf{h}(\xi)\mathbf{B}_0$ given by

$$\mathbf{h}(\xi) = \begin{bmatrix} 1 & \xi & \xi^2 \end{bmatrix}, \tag{51}$$

$$\begin{bmatrix} \mathbf{h}(-1) \\ \mathbf{h}(0) \\ \mathbf{h}(1) \end{bmatrix} \mathbf{B_0} = \mathbf{I}. \tag{52}$$

4.1. Geometry and coordinate transformations

The cross-section's midsurface is interpolated with the quadratic shape functions. Thus, it's location in a Cartesian coordinate system is given by

$$\mathbf{r}_m = \begin{bmatrix} X_m & Y_m\cos\phi & Y_m\sin\phi \end{bmatrix}^{\mathrm{T}}, \tag{53}$$

$$X_m = \mathbf{h}\mathbf{b}_x, \quad Y_m = \mathbf{h}\mathbf{b}_r, \quad \mathbf{b}_x = \mathbf{B_0}\begin{bmatrix} X_1 \\ X_2 \\ X_3 \end{bmatrix}, \quad \mathbf{b}_r = \mathbf{B_0}\begin{bmatrix} Y_1 \\ Y_2 \\ Y_3 \end{bmatrix}, \tag{54}$$

where (X_i, Y_i) is the location of node i, for $\phi = 0$.

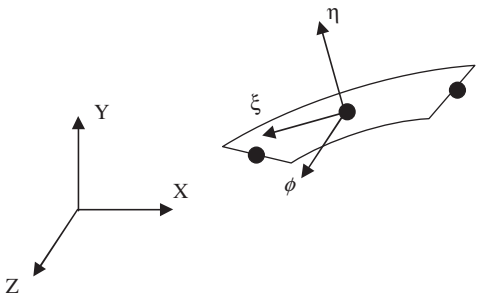

Fig. 2. Sketch of shell element. Dots show the node locations. Global coordinate system is defined by the coordinates X, Y and Z. Local coordinate system is defined by curvilinear coordinates, ξ, ϕ and η.

The midsurface of the waveguide element is defined by the coordinates ξ and ϕ. Following [18, Eq. (1.2)] we define the tangent vectors

$$\mathbf{r}_{m,\xi} = \frac{\partial \mathbf{r}_m}{\partial \xi} = \begin{bmatrix} X'_m & Y'_m \cos\phi & Y'_m \sin\phi \end{bmatrix}^{\mathrm{T}},$$
$$\mathbf{r}_{m,\phi} = \frac{\partial \mathbf{r}_m}{\partial \phi} = \begin{bmatrix} 0 & -Y_m \sin\phi & Y_m \cos\phi \end{bmatrix}^{\mathrm{T}} \tag{55}$$

and the length scales

$$A = |\mathbf{r}_{m,\xi}| = \sqrt{(X'_m)^2 + (Y'_m)^2}, \quad B = |\mathbf{r}_{m,\phi}| = |Y_m|, \tag{56}$$

where prime denotes differentiation with respect to ξ. It is apparent that the vectors in Eq. (55) are orthogonal and the following orthonormal vectors are defined:

$$\mathbf{e}_\xi = \mathbf{r}_{m,\xi}/A, \quad \mathbf{e}_\phi = \mathbf{r}_{m,\phi}/B,$$
$$\mathbf{e}_\eta = \mathbf{e}_\xi \times \mathbf{e}_\phi = \begin{bmatrix} Y'_m Y_m & -X'_m Y_m \cos\phi & -X'_m Y_m \sin\phi \end{bmatrix}^{\mathrm{T}}/AB, \tag{57}$$

where $\times$ denotes vector product.

The following quantities are also defined:

$$N_1 = \mathbf{r}^{\mathrm{T}}_{m,\xi\xi}\mathbf{e}_\eta, \quad N_2 = \mathbf{r}^{\mathrm{T}}_{m,\phi\phi}\mathbf{e}_\eta, \tag{58}$$

where

$$\mathbf{r}_{m,\xi\xi} = \frac{\partial^2 \mathbf{r}_m}{\partial \xi^2} = \begin{bmatrix} X''_m & Y''_m \cos\phi & Y''_m \sin\phi \end{bmatrix}^{\mathrm{T}},$$
$$\mathbf{r}_{m,\phi\phi} = \frac{\partial^2 \mathbf{r}_m}{\partial \phi^2} = \begin{bmatrix} 0 & -Y_m \cos\phi & -Y_m \sin\phi \end{bmatrix}^{\mathrm{T}}. \tag{59}$$

Upon this basis, the surface's radii of curvatures are given by Leissa [18, Eq. (1.15)]

$$\frac{1}{R_\xi} = -\frac{N_1}{A^2} = \frac{Y_m(Y''_m X'_m - X''_m Y'_m)}{A^3 B}, \quad \frac{1}{R_\phi} = -\frac{N_2}{B^2} = -\frac{X'_m}{AB}. \tag{60}$$

It is noted that R_ξ, R_ϕ, A and B are functions of ξ only, which concludes the geometry specification.

4.2. Displacements

Adopting Navier's assumption, the displacement, $\mathbf{u}$, in the local system is given by the displacement at the midsurface and rotations about the $\mathbf{e}_\xi$ and $\mathbf{e}_\phi$ axes

$$\mathbf{u} = \begin{bmatrix} \mathbf{u}^{\mathrm{T}}\mathbf{e}_\xi \\ \mathbf{u}^{\mathrm{T}}\mathbf{e}_\eta \\ \mathbf{u}^{\mathrm{T}}\mathbf{e}_\phi \end{bmatrix} = \begin{bmatrix} u + \eta\beta \\ v \\ w - \eta\alpha \end{bmatrix}, \tag{61}$$

where α and β are the rotations about the $\mathbf{e}_\xi$ and $\mathbf{e}_\phi$ axes, respectively. The mid-surface displacements in Eq. (61) are interpolated with the quadratic shape functions $\mathbf{hB}_0$:

$$u = \mathbf{hB}_u\mathbf{v}, \quad v = \mathbf{hB}_v\mathbf{v}, \quad w = \mathbf{hB}_w\mathbf{v}, \quad \alpha = \mathbf{hB}_\alpha\mathbf{v}, \quad \beta = \mathbf{hB}_\beta\mathbf{v}, \tag{62}$$

where $\mathbf{v}$ contains the nodal displacements. Taking the nodal degrees of freedom as the three displacements and the three rotations, we have

$$\mathbf{v} = \begin{bmatrix} \mathbf{v}_1 \\ \mathbf{v}_2 \\ \mathbf{v}_3 \end{bmatrix}, \quad \mathbf{v}_i = \begin{bmatrix} u_i & v_i & w_i & \alpha_i & \chi_i & \beta_i \end{bmatrix}^{\mathrm{T}}, \tag{63}$$

where χ is the rotation about the $\mathbf{e}_n$ axis. The 3×18 matrices $\mathbf{B}_u$, $\mathbf{B}_v$, etc, each have three non-zero columns, which are those of $\mathbf{B}_0$. The locations of these columns are given by the order of the nodal degrees of freedom in $\mathbf{v}$. Thus, as an example, the 1st, 7th and 13th columns of $\mathbf{B}_u$ equals the three columns of $\mathbf{B}_0$.

4.3. Strain–displacement relations

Following Leissa's derivation of the strain to displacement relations, the engineering strain vector is given by Leissa [18, Eqs. (1.41), (1.42), (1.36e) and (1.36f)]

$$\boldsymbol{\varepsilon} = \begin{bmatrix} \varepsilon_\xi & \varepsilon_\phi & \gamma_{\xi\phi} & \kappa_\xi & \kappa_\phi & \tau & \gamma_{\xi\eta} & \gamma_{\phi\eta} \end{bmatrix}^{\mathrm{T}}, \tag{64}$$

where

$$\varepsilon_\xi = \frac{1}{A}\frac{\partial u}{\partial \xi} + \frac{v}{R_\xi} + \frac{w}{AB}\frac{\partial A}{\partial \phi}, \quad \varepsilon_\phi = \frac{u}{AB}\frac{\partial B}{\partial \xi} + \frac{v}{R_\phi} + \frac{1}{B}\frac{\partial w}{\partial \phi}, \quad \gamma_{\xi\phi} = \frac{A}{B}\frac{\partial (u/A)}{\partial \phi} + \frac{B}{A}\frac{\partial (w/B)}{\partial \xi}, \tag{65}$$

$$\kappa_\xi = -\frac{\alpha}{AB}\frac{\partial A}{\partial \phi} + \frac{1}{A}\frac{\partial \beta}{\partial \xi}, \quad \kappa_\phi = -\frac{1}{B}\frac{\partial \alpha}{\partial \phi} + \frac{\beta}{AB}\frac{\partial B}{\partial \xi},$$

$$\tau = -\frac{B}{A}\frac{\partial (\alpha/B)}{\partial \xi} + \frac{A}{B}\frac{\partial (\beta/A)}{\partial \phi} + \frac{1}{R_\xi}\left(\frac{1}{B}\frac{\partial u}{\partial \phi} - \frac{w}{AB}\frac{\partial B}{\partial \xi}\right) + \frac{1}{R_\phi}\left(\frac{1}{A}\frac{\partial w}{\partial \xi} - \frac{u}{AB}\frac{\partial A}{\partial \phi}\right), \tag{66}$$

$$\gamma_{\xi\eta} = \frac{1}{A}\frac{\partial v}{\partial \xi} - \frac{u}{R_\xi} + \beta, \quad \gamma_{\phi\eta} = \frac{1}{B}\frac{\partial v}{\partial \phi} - \frac{w}{R_\phi} - \alpha. \tag{67}$$

The expressions for the transverse shear in Eqs. (67) are not given in Ref. [18] but follows if terms of the order of η/R_ξ and η/R_ϕ in Ref. [18, Eqs. (1.36e) and (1.36f)] are neglected compared to unity. Expressions (65)–(67) are identical to those given by Washizu [27, Eq. (9.79)], except for that the radii of curvature appear to be defined positive in the opposite direction. Now, the displacement (62) are inserted into Eq. (64) and the strain vector is partitioned as in Eq. (29) where, keeping in mind that A and B do not depend on ϕ,

$$\mathbf{E}_0 = \begin{bmatrix} \mathbf{h}'\mathbf{B}_u/A + \mathbf{h}\mathbf{B}_v/R_\xi \\ \mathbf{h}\mathbf{B}_u B_p + \mathbf{h}\mathbf{B}_v/R_\phi \\ \mathbf{h}'\mathbf{B}_w/A - \mathbf{h}\mathbf{B}_w B_p \\ \mathbf{h}'\mathbf{B}_\beta/A \\ \mathbf{h}\mathbf{B}_\beta B_p \\ \mathbf{h}'(-\mathbf{B}_\alpha + \mathbf{B}_w/R_\phi)/A + \mathbf{h}(\mathbf{B}_\alpha - \mathbf{B}_w/R_\xi)B_p \\ \mathbf{h}'\mathbf{B}_v/A + \mathbf{h}\mathbf{B}_\beta - \mathbf{h}\mathbf{B}_u/R_\xi \\ -\mathbf{h}\mathbf{B}_\alpha - \mathbf{h}\mathbf{B}_w/R_\phi \end{bmatrix}, \quad \mathbf{E}_1 = \frac{1}{B}\begin{bmatrix} 0 \\ \mathbf{h}\mathbf{B}_w \\ \mathbf{h}\mathbf{B}_u \\ 0 \\ -\mathbf{h}\mathbf{B}_\alpha \\ \mathbf{h}(\mathbf{B}_u/R_\xi + \mathbf{B}_\beta) \\ 0 \\ \mathbf{h}\mathbf{B}_v \end{bmatrix}, \tag{68}$$

$$B_p = B'/(AB) = Y'_m Y_m/AB^2. \tag{69}$$

4.4. Strain and kinetic potential

The kinetic potential is given by

$$\begin{aligned} \bar{K} &= \int_V -\omega^2 \mathbf{u}^{a\mathrm{T}} \rho \mathbf{u}\, \mathrm{d}V \\ &= \int\int_{-1}^{1}\int_{-h/2}^{h/2} -\omega^2 \mathbf{u}^{a\mathrm{T}} \rho \mathbf{u} A(1+\eta/R_\xi)B(1+\eta/R_\phi)\, \mathrm{d}\eta\, \mathrm{d}\xi \mathrm{d}\phi, \end{aligned} \tag{70}$$

where h is the wall-thickness.

The expressions for displacement (61) are inserted into this expression and the integrals are evaluated neglecting the change of arc length through the thickness, as is standard in, e.g., Love's shell theory. Thus, the

kinetic potential is as follows:

$$\bar{K} = \int -\omega \mathbf{v}^{a\mathrm{T}}(\mathbf{B}_u^{\mathrm{H}}\mathbf{M}_0\mathbf{B}_u + \mathbf{B}_v^{\mathrm{H}}\mathbf{M}_0\mathbf{B}_v + \mathbf{B}_w^{\mathrm{H}}\mathbf{M}_0\mathbf{B}_w + h^2/12(\mathbf{B}_\alpha^{\mathrm{H}}\mathbf{M}_0\mathbf{B}_\alpha + \mathbf{B}_\beta^{\mathrm{H}}\mathbf{M}_0\mathbf{B}_\beta))\mathbf{v}\,\mathrm{d}\phi, \tag{71}$$

$$\mathbf{M}_0 = \int_{-1}^{1} \rho h \mathbf{h}^{\mathrm{T}}\mathbf{h} AB\,\mathrm{d}\xi. \tag{72}$$

The strain potential is best described in the local coordinate system. It is given by

$$\bar{U} = \int \int_{-1}^{1} \boldsymbol{\varepsilon}^{a\mathrm{T}}\mathbf{D}\boldsymbol{\varepsilon} AB\,\mathrm{d}\xi\,\mathrm{d}\phi. \tag{73}$$

Now, the strain expressions are inserted into Eq. (73), upon which it follows that

$$\bar{U} = \int \sum_{n=0}^{1}\sum_{m=0}^{1} \frac{\partial^n \mathbf{v}^{a\mathrm{T}}}{\partial \phi^n}\left(\int_{-1}^{1} \mathbf{E}_n^{\mathrm{H}}\mathbf{D}\mathbf{E}_m AB\,\mathrm{d}\xi\right)\frac{\partial^m \mathbf{v}}{\partial \phi^m}\,\mathrm{d}\phi. \tag{74}$$

The nodal displacements at node i, $\mathbf{V}_i$, expressed by the global coordinates and $\mathbf{v}_i$, expressed by the local coordinates are related by

$$\mathbf{V}_i = \begin{bmatrix} \begin{bmatrix} \mathbf{e}_\xi & \mathbf{e}_\eta & \mathbf{e}_\phi \end{bmatrix} & 0 \\ 0 & \begin{bmatrix} \mathbf{e}_\xi & \mathbf{e}_\eta & \mathbf{e}_\phi \end{bmatrix} \end{bmatrix} \mathbf{v}_i. \tag{75}$$

4.4.1. The rigidity matrix

For a homogenous material, and neglecting the trapezoidal shape of the cross section for a curved structure

$$\mathbf{D} = \begin{bmatrix} \mathbf{D}_{00} & \mathbf{D}_{01} & 0 & 0 \\ \mathbf{D}_{10} & \mathbf{D}_{11} & 0 & 0 \\ 0 & 0 & D_s & 0 \\ 0 & 0 & 0 & D_s \end{bmatrix}, \tag{76}$$

$$\mathbf{D}_{nm} = \int_{-h/2}^{h/2} \mathbf{D}_0 \eta^{(n+m)}\,\mathrm{d}\eta. \tag{77}$$

If the material is also isotropic, we have

$$\mathbf{D_0} = \frac{E}{1-v^2}\begin{bmatrix} 1 & v & 0 \\ v & 1 & 0 \\ 0 & 0 & (1-v)/2 \end{bmatrix}, \tag{78}$$

where E is Young's modulus and v is Poisson's ratio. Thus, for a cross section in which the rigidity is independent of η, it follows that

$$\mathbf{D}_{01} = \mathbf{D}_{10} = 0, \quad \mathbf{D}_{00} = h\mathbf{D}_0, \quad \mathbf{D}_{11} = \frac{h^3}{12}\mathbf{D}_0, \tag{79}$$

$$D_s = hE/2k(1+v). \tag{80}$$

The factor k, included in the shear term, is taken as $6/5$ and its purpose is to improve the shear displacement approximation.

The way to handle a pre-loaded curved shell, which is needed to model inflated car tyres, is presented in Appendix C.

5. Elements for straight waveguides

Elements for straight waveguides are obviously less complicated than the elements for curved waveguides, but they are derived in exactly the same way. An abreviated derivation for straight waveguides will now follow.

5.1. Straight isoparametic solid waveguide finite element

The derivation is completely analogous to the element derived in Section 3. However, the following alterations must be made. In Eqs. (38), (39), (44) and (45) r will be replaced by y. In Eq. (40) ϕ will be replaced by z.

The main difference is that the strain displacement relations are changed meaning that Eqs. (41)–(43) will be replaced by

$$\boldsymbol{\varepsilon} = \begin{bmatrix} \varepsilon_x & \varepsilon_y & \varepsilon_z & \gamma_{xy} & \gamma_{xz} & \gamma_{yz} \end{bmatrix}^{\mathrm{T}}, \tag{81}$$

$$\begin{aligned} &\varepsilon_x = \frac{\partial u}{\partial x}, \quad \varepsilon_y = \frac{\partial v}{\partial y}, \quad \varepsilon_z = \frac{\partial w}{\partial z}, \\ &\gamma_{xy} = \frac{\partial v}{\partial x} + \frac{\partial u}{\partial y}, \quad \gamma_{xz} = \frac{\partial w}{\partial x} + \frac{\partial u}{\partial z}, \quad \gamma_{yz} = \frac{\partial w}{\partial y} + \frac{\partial v}{\partial z}, \end{aligned} \tag{82}$$

$$\mathbf{E}_0 = \begin{bmatrix} \mathbf{h}_x\mathbf{B}_u \\ \mathbf{h}_y\mathbf{B}_v \\ 0 \\ \mathbf{h}_x\mathbf{B}_v + \mathbf{h}_y\mathbf{B}_u \\ \mathbf{h}_x\mathbf{B}_w \\ \mathbf{h}_y\mathbf{B}_w \end{bmatrix}, \quad \mathbf{E}_1 = \begin{bmatrix} 0 \\ 0 \\ \mathbf{h}\mathbf{B}_w \\ 0 \\ \mathbf{h}\mathbf{B}_u \\ \mathbf{h}\mathbf{B}_v \end{bmatrix}. \tag{83}$$

In the first line of the Lagrangian, Eq. (47), $r\,\mathrm{d}\phi$ will be replaced by $\mathrm{d}z$ and in the second line ϕ will be replaced by z. Thus, the factor r is ommitted in Eqs. (48) and (50).

5.2. Straight isoparametic single-curved deep-shell waveguide finite element

In the limit of infinite radius of curvature ($1/R_\phi \to 0$) the element becomes straight. The derivation is completely analogous to Section 4 but with the following alterations.

Eqs. (53), (55), (56), (57), (59) and (60) will be replaced by

$$\mathbf{r}_m = \begin{bmatrix} X_m & Y_m & z \end{bmatrix}^{\mathrm{T}}, \tag{84}$$

$$\begin{aligned} \mathbf{r}_{m,\xi} &= \frac{\partial \mathbf{r}_m}{\partial \xi} = \begin{bmatrix} X'_m & Y'_m & 0 \end{bmatrix}^{\mathrm{T}}, \\ \mathbf{r}_{m,z} &= \frac{\partial \mathbf{r}_m}{\partial z} = \begin{bmatrix} 0 & 0 & 1 \end{bmatrix}^{\mathrm{T}}, \end{aligned} \tag{85}$$

$$A = |\mathbf{r}_{m,\xi}| = \sqrt{(X'_m)^2 + (Y'_m)^2}, \quad B = |\mathbf{r}_{m,z}| = |1|, \tag{86}$$

$$\begin{aligned} &\mathbf{e}_\xi = \mathbf{r}_{m,\xi}/A, \quad \mathbf{e}_z = \mathbf{r}_{m,z}/B. \\ &\mathbf{e}_\eta = \mathbf{e}_\xi \times \mathbf{e}_z = \begin{bmatrix} Y'_m & X'_m & 0 \end{bmatrix}^{\mathrm{T}}/AB, \end{aligned} \tag{87}$$

$$\mathbf{r}_{m,\xi\xi} = \frac{\partial^2 \mathbf{r}_m}{\partial \xi^2} = \begin{bmatrix} X''_m & Y''_m & 0 \end{bmatrix}^{\mathrm{T}},$$
$$\mathbf{r}_{m,zz} = \frac{\partial^2 \mathbf{r}_m}{\partial z^2} = \begin{bmatrix} 0 & 0 & 0 \end{bmatrix}^{\mathrm{T}}, \tag{88}$$

$$\frac{1}{R_\xi} = \frac{(Y''_m X'_m - X''_m Y'_m)}{A^3 B}, \quad \frac{1}{R_z} = 0. \tag{89}$$

In Eq. (54) r will be replaced by y and in Eqs. (58) and (61) ϕ will be replaced by z. This leads to some simplifications since the terms involving $(1/R_z)$ vanish. Eqs. (64)–(68) are replaced by the following relations:

$$\varepsilon = \begin{bmatrix} \varepsilon_\xi & \varepsilon_z & \gamma_{\xi z} & \kappa_\xi & \kappa_z & \tau & \gamma_{\xi\eta} & \gamma_{z\eta} \end{bmatrix}^{\mathrm{T}}, \tag{90}$$

where

$$\varepsilon_\xi = \frac{1}{A}\frac{\partial u}{\partial \xi} + \frac{v}{R_\xi} + \frac{w}{AB}\frac{\partial A}{\partial z}, \quad \varepsilon_z = \frac{u}{AB}\frac{\partial B}{\partial \xi} + \frac{1}{B}\frac{\partial w}{\partial z},$$
$$\gamma_{\xi z} = \frac{A}{B}\frac{\partial (u/A)}{\partial z} + \frac{B}{A}\frac{\partial (w/B)}{\partial \xi}, \tag{91}$$

$$\kappa_\xi = -\frac{\alpha}{AB}\frac{\partial A}{\partial z} + \frac{1}{A}\frac{\partial \beta}{\partial \xi}, \quad \kappa_z = -\frac{1}{B}\frac{\partial \alpha}{\partial z} + \frac{\beta}{AB}\frac{\partial B}{\partial \xi},$$
$$\tau = -\frac{B}{A}\frac{\partial (\alpha/B)}{\partial \xi} + \frac{A}{B}\frac{\partial (\beta/A)}{\partial z} + \frac{1}{R_\xi}\left(\frac{1}{B}\frac{\partial u}{\partial z} - \frac{w}{AB}\frac{\partial B}{\partial \xi}\right), \tag{92}$$

$$\gamma_{\xi\eta} = \frac{1}{A}\frac{\partial v}{\partial \xi} - \frac{u}{R_\xi} + \beta, \quad \gamma_{z\eta} = \frac{1}{B}\frac{\partial v}{\partial z} - \alpha, \tag{93}$$

$$\mathbf{E}_0 = \begin{bmatrix} \mathbf{h}'\mathbf{B}_u/A + \mathbf{h}\mathbf{B}_v/R_\xi \\ 0 \\ \mathbf{h}'\mathbf{B}_w/A \\ \mathbf{h}'\mathbf{B}_\beta/A \\ 0 \\ -\mathbf{h}'\mathbf{B}_\alpha/A \\ \mathbf{h}'\mathbf{B}_v/A + \mathbf{h}\mathbf{B}_\beta - \mathbf{h}\mathbf{B}_u/R_\xi \\ -\mathbf{h}\mathbf{B}_\alpha \end{bmatrix}, \quad \mathbf{E}_1 = \frac{1}{B}\begin{bmatrix} 0 \\ \mathbf{h}\mathbf{B}_w \\ \mathbf{h}\mathbf{B}_u \\ 0 \\ -\mathbf{h}\mathbf{B}_\alpha \\ \mathbf{h}(\mathbf{B}_u/R_\xi + \mathbf{B}_\beta) \\ 0 \\ \mathbf{h}\mathbf{B}_v \end{bmatrix}. \tag{94}$$

In Eqs. (70), (71) and (73)–(75) ϕ should be replaced with z.

6. Numerical example

The elements developed in this work are in Ref. [12] used to model the vibration of a car tyre, which is a complex, composite structure with anisotropic material properties. Here, a simple example is considered to illustrate the procedures and the applications of waveguide FE in an assumed modes procedure. This example considers an isotropic circular cylinder of length L, radius R and thickness h, see Fig. 3, where also a cylindrical coordinate system $[x, r, \theta]$ and a Cartesiean coordinate system $[x, y, z]$ are indicated. The boundary conditions at the cylinder ends are referred to as "shear diaphragm" conditions, meaning that the displacements in the cross-sectional plane are blocked while the displacements along the

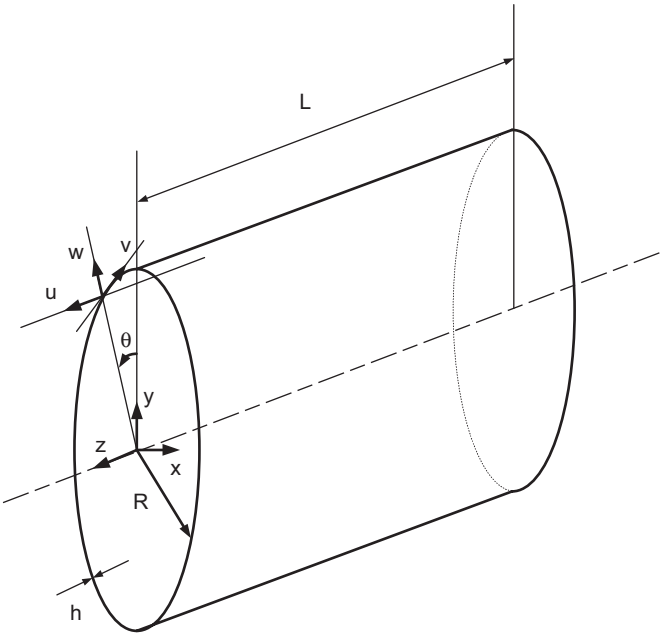

Fig. 3. Coordinate systems and definition of directions. u, v and w are the displacements in the axial, circumferential and radial directions, respectively.

cylinder axis are free:

$$v(0) = v(L) = 0,$$
$$w(0) = w(L) = 0, \tag{95}$$

where v and w are the displacements in the circumferential and radial direction, respectively.

One advantage of the example structure is that the "exact" results presented by Leissa [18 Table 2.8] can be used for validation. Another advantage is that all four elements presented in this work can model the vibration field. Thus Fig. 4 show the mesh for a straight waveguide modelled with the deep shell elements presented in Section 5.2. Fig. 5 show the mesh for a straight waveguide modelled with the solid element presented in Section 5.1. In this mesh three elements on top of each other are used to accurately model the shear deformation across the shell thickness. Fig. 6 show the mesh for the doubly curved deep shell elements presented in Section 4. Finally, Fig. 7 show the mesh for the curved solid elements presented in Section 3.

The meshes displayed in the figures considers a cylinder of length $L = 1\,\mathrm{m}$ and radius $R = 1\,\mathrm{m}$, while different size cylinders are considered in the calculations.

6.1. Thin shell theory

In thin shell theory the displacement functions that fully satisfy the shear diaphragm end conditions are given by

$$u = A\cos\lambda z\cos n\theta\cos\omega t,$$
$$v = B\sin\lambda z\sin n\theta\cos\omega t,$$
$$w = C\sin\lambda z\cos n\theta\cos\omega t, \tag{96}$$

where u, v and w are the displacements in the axial, circumferential and radial direction, respectively, see Fig. 3. A, B and C are undetermined constants. ω is the angular frequency, λ is the axial wavenumber and n is the circumferential wave order. The latter is always an integer.

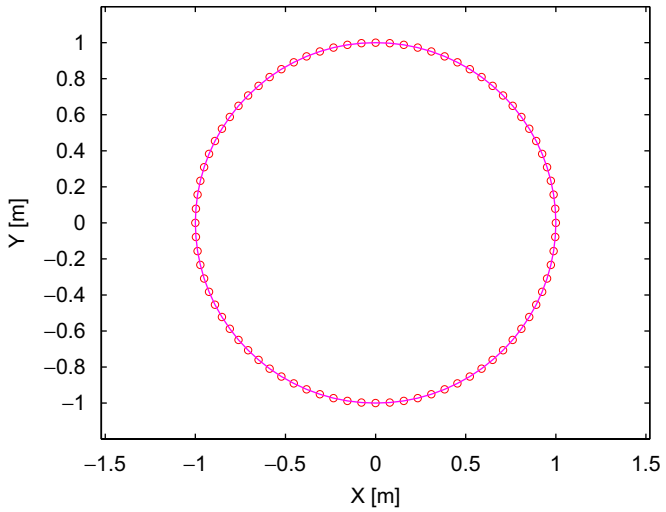

Fig. 4. Straight deep shell element mesh. The mesh has 80 nodes and 40 elements.

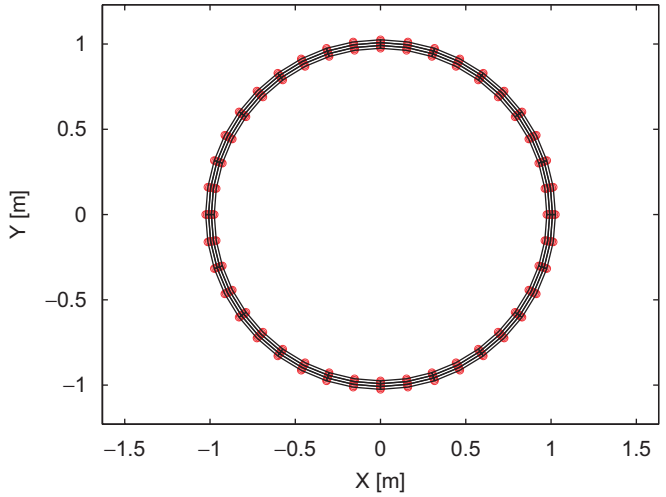

Fig. 5. Straight solid element mesh. The mesh has 280 nodes and 60 elements.

The displacement function are inserted into any thin shell theory leading to an eigenvalue problem [18] and a non-trivial solution ω is sought for given values of circumferential wave order, n, and axial wavenumber λ.

To satisfy the shear diaphragm end conditions the axial wavenumber λ must be given by

$$\lambda = \frac{m\pi}{L} \quad (m = 1, 2, ...), \tag{97}$$

where L is the length of the cylinder and m is an integer.

6.2. Straight waveguide

For a straight waveguide the differential equation is given by (compare with Eq. (32))

$$\mathbf{K}_2 \frac{\partial^2 \tilde{\mathbf{v}}}{\partial z^2} + \mathbf{K}_1 \frac{\partial \tilde{\mathbf{v}}}{\partial z} + \mathbf{K}_0 \tilde{\mathbf{v}} - \omega^2 \mathbf{M} \tilde{\mathbf{v}} = 0. \tag{98}$$

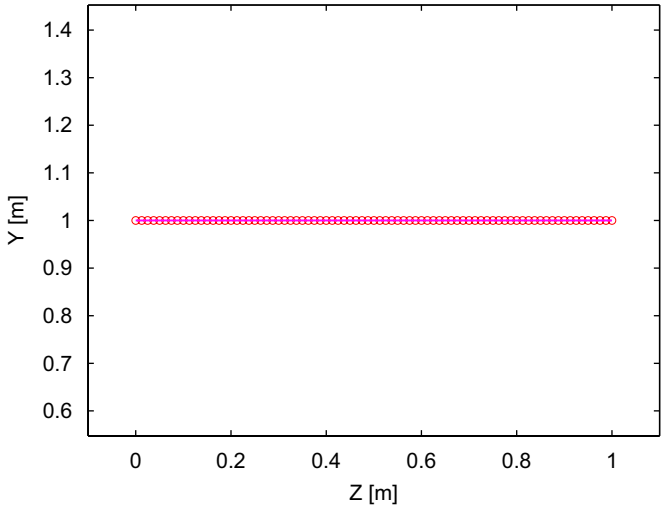

Fig. 6. Curved deep shell element mesh. The mesh has 81 nodes and 40 elements.

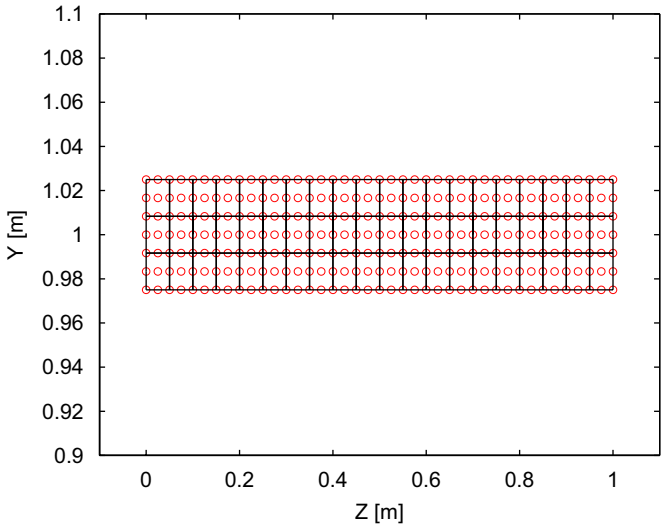

Fig. 7. Curved solid element mesh. The mesh has 287 nodes and 60 elements.

A solution of the form $\tilde{\mathbf{v}} = \tilde{\mathbf{v}}_n \, \mathrm{e}^{\mathrm{i}\lambda z}$ is assumed leading to

$$(-\mathbf{K}_2\lambda^2 + \mathrm{i}\lambda\mathbf{K}_1 + \mathbf{K}_0\tilde{\mathbf{v}} - \omega^2\mathbf{M})\tilde{\mathbf{v}} = 0. \tag{99}$$

By solving Eq. (99) for different values of axial waveorder, λ, a dispersion curve is generated, see Fig. 8 where the values on the y-axis corresponds to axial waveorder, and the x-axis correspond to non-dimensional frequency Ω:

$$\Omega^2 = \frac{\rho(1-\nu^2)}{E} R^2\omega^2, \tag{100}$$

where R is the radius, ρ is the density, ν is Poisson's ratio and E is Young's modulus.

The dispersion curve consists of different branches, each with its own characteristic mode shape determined by the circumferential waveorder n.

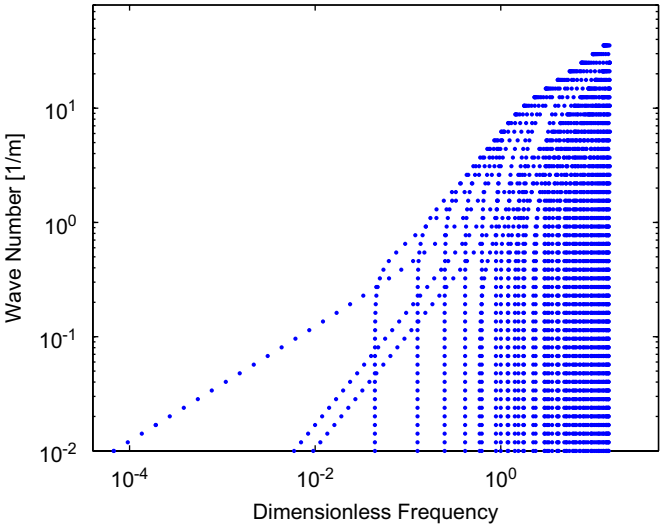

Fig. 8. Dispersion curve for the cylinder. The wavenumber refers to axial wave number λ. The dimensionless frequency is defined in Eq. (100).

The first branch from the bottom left corresponds to a bending wave similar to the one given by Euler beam theory. For this family $n = 1$, see Fig. 9(a). The second and third branches are axi symmetric families ($n = 0$), in this case torsional and longitudinal modes, respectively, see Figs. 9(b) and (c). Branch number four, five and six correspond to radial-axial waves with a circumferential wave order of $n = 2, n = 3$ and $n = 4$. In these cases waves with two, three and four wavelengths are travelling around the cylinder in the circumferential direction, see Figs. 9(d)–(f).

Leissa presents results for given n and L/mR ratios. To compare with Leissa's results the ratio L/mR is given, L and R are fixed, leading to m. Now, $\lambda = m\pi/L$ is inserted into Eq. (99), and the frequency is solved for. The correct mode is then identified via its modeshape, which is quite similar to those in Eq. (96).

6.3. Curved waveguide

When the elements for curved waveguides, derived in Sections 3 and 4, are used the boundary conditions at the cylinder ends have to be explicitly imposed. For the deep shell elements mesh this means that for the edge nodes the displacement in the radial and circumferential direction and the rotation about the x-axis are blocked. For the solid elements the displacements at $z = 0$ and $z = L$, in the radial and circumferential directions, are blocked.

For a curved waveguide, Eq. (32) is valid when no external forces are present, it is here restated:

$$\mathbf{K}_2 \frac{\partial^2 \tilde{\mathbf{v}}}{\partial \phi^2} + \mathbf{K}_1 \frac{\partial \tilde{\mathbf{v}}}{\partial \phi} + \mathbf{K}_0 \tilde{\mathbf{v}} - \omega^2 \mathbf{M} \tilde{\mathbf{v}} = 0. \tag{101}$$

A solution of the form $\tilde{\mathbf{v}} = \tilde{\mathbf{v}}_n e^{in\phi}$ is assumed leading to the following eigenvalue problem:

$$(-n^2 \mathbf{K}_2 + i n \mathbf{K}_1 + \mathbf{K}_0 - \omega^2 \mathbf{M}) \tilde{\mathbf{v}}_n = 0. \tag{102}$$

To compare with Leissa, L/mR is given, L and m are fixed, leading to R. The eigenvalue problem (Eq. (102)) is solved for given integer values of circumferential waveorder n. m is fixed to equal 1 meaning that the mode to be identified is the one with half a wavelength in the axial direction, see Fig. 10.

6.4. Results

The results are, as mentioned before, presented by Leissa as triples $[L/mRn\Omega]$ for two radius to thickness ratios ($R/h = 20$ and $R/h = 500$). The results are mainly obtained with three-dimensional elasticity theory.

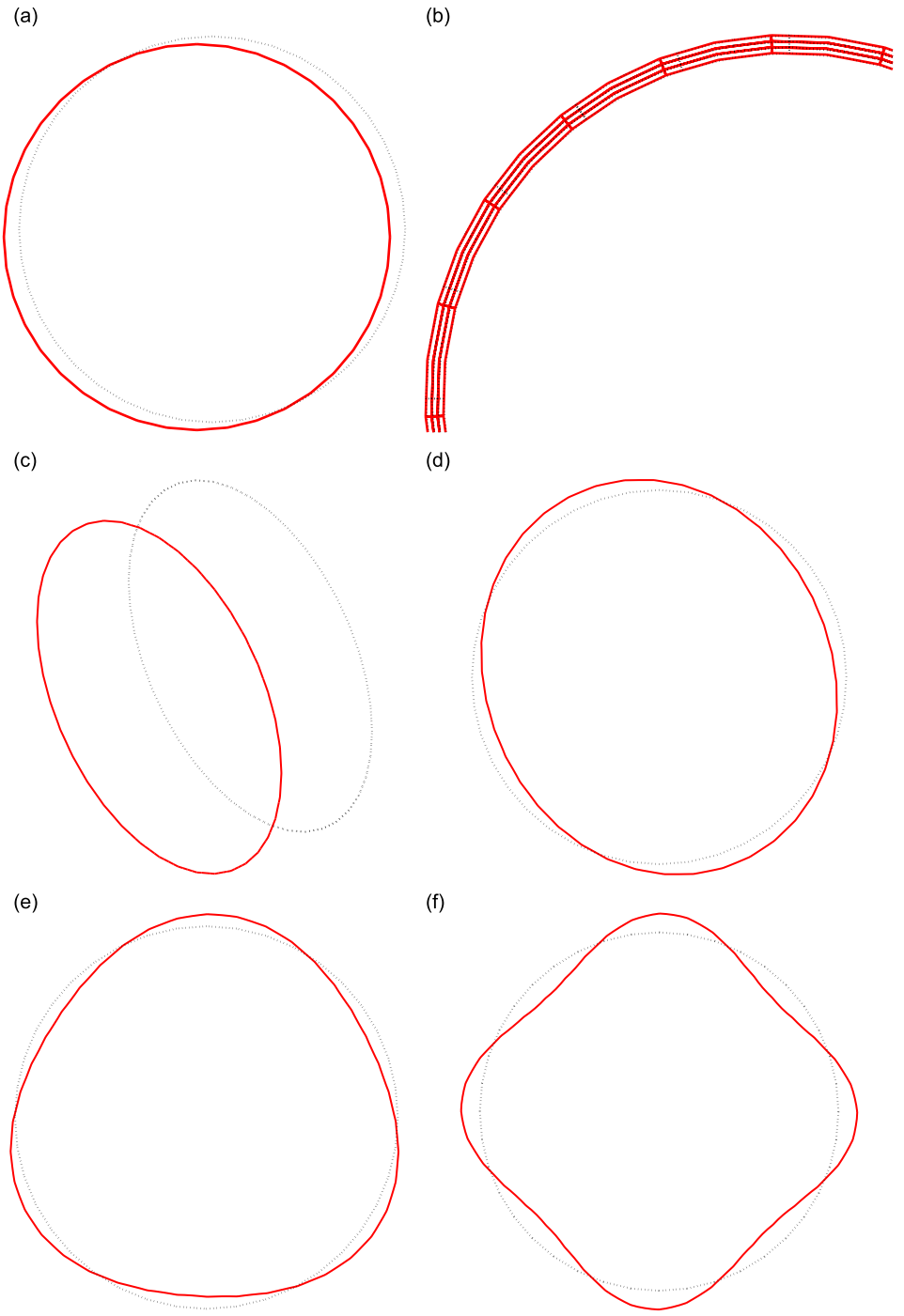

Fig. 9. Mode shapes corresponding to the six first branches, from left to right, at the bottom in Fig. 8. (a) Bending wave, $n = 1$; (b) torsional wave, $n = 0$; (c) longitudinal wave, $n = 0$; (d) radial-axial wave, $n = 2$; (e) radial-axial wave, $n = 3$; (f) radial-axial wave, $n = 4$.

For some parameter combination for the very thin shell Flugge theory [18] is used instead. There seems to be an error in the presented tables. The value of Ω for $[L/mR = 100, n = 1, R/h = 500]$ is given as $\Omega = 0.002664824$ but when the calculation is checked with Warburton shell theory, [18, Section 2.2.2], the result is $\Omega = 0.0006648237$. According to Leissa the error in this estimation compared to three-dimensional elasticity

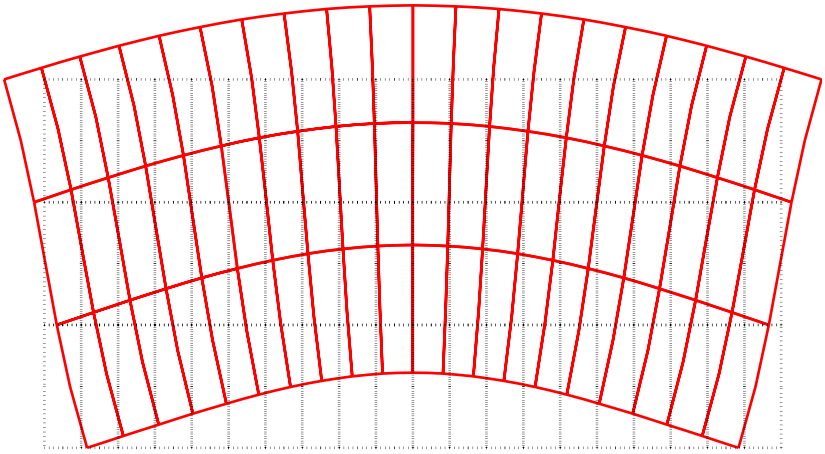

Fig. 10. Typical mode shape when the curved waveguide is considered. $R/h = 20$, $L/mR = 0.1$, $n = 2$, $m = 1$, leading to half a wavelength in the axial direction. $\Omega = 10.7034$.

theory should be less than 0.01% [18, Table 2.7]. This means that there is at least one error in the tables and since the Warburton value agrees better with results in this study it is assumed correct.

First, the thick case $R/h = 20$ is discussed. The results are presented in tables where Leissa's results are compared to the waveguide FE results one mode family at the time. All of Leissa's cases have been considered, but for simplicity some of Leissa's results are omitted. The results presented here are typical in terms of relative error.

When the straight waveguide with deep shell elements is considered a shear and membrane locking problem can appear. This is described in for example [28, Section 13.4]. The consequence is that the bending wave family and the torsional mode family are not propagated below certain "cut-on" frequencies, which is not correct. By increasing the level of interpolation in the elements, by increasing the number of nodes or the polynomial degree of the shape function, the "cut-on" can be lowered in terms of frequency but never completely avoided. One remedy is reduced integration for the membrane and transverse shear terms [28, Section 15.4]. Another remedy is to put the middle node in the element on the straight line between the edge nodes: this turns the mesh into a facet structure. Both of these methods give satisfactory results.

Tables 1 and 2 present the results for the zero-order mode and the bending mode for different meshes. Except for the case $L/mR = 0.1$ the results are very good.

Table 3 displays the results for the fourth-order radial axial mode for different meshes. An increased number of nodes are needed to correctly describe the dynamic behaviour of this mode family. When the straight waveguide with 60 solid elements, in three layers, is used there are 40 nodes in the circumferential direction which is insufficient (error 18.89% for $L/mR = 100$). By increasing the number of nodes around the cylinder the problem is avoided. This is not a problem for the curved waveguide since the wave motion around the cylinder is exactly modelled.

When the cylinders are short and chubby, $L/mR = 0.1$, there seem to be a systematic error. This error is around one percent for the deep shell elements and around two percent for the solid elements regardless if the waveguide is straight or curved.

It should also be noted that one layer of solid elements are as good as three layers. The reason is probably that the considered modes are rather simple, and to accurately capture the shearing of the cross section is not important.

For the thin cylinder case, $R/h = 500$, radial axial modes up to the order of $n = 25$ are located at lower frequencies than the modes of interest for some L/mR ratios. High-order modes require many elements to be described accurately (the lower theoretical limit is two nodes per wavelength in analogy with the Nyquist frequency). Usually the mode order increases with frequency but shells are complex. In this case, 40 elements are insufficient but 80 elements are enough, for the straight waveguide deep shell mesh. This problem does not concern the curved waveguide.

Table 1
Zero-order modes ($n = 0$) for $R/h = 20$

	L/mR		
	0.1	4	100
Dimensionless frequency [18]	10.4586	0.464648	0.0185859
Error in percent			
Straight waveguide, 40 deep shell elements	1.03	0.03	0.03
Straight waveguide, 20 solid elements 1 layer	4.15	b	b
Straight waveguide, 60 solid elements 3 layers	2.02	b	b
Straight waveguide, 120 solid elements 3 layers	2.02	b	b
Curved waveguide, 40 deep shell elements	1.03	0.03	0.03
Curved waveguide, 60 solid elements 3 layers	2.02	b	b

Values are the error compared to Leissa [18] in percent. b indicates differences smaller than 0.01 percent.

Table 2
Bending modes ($n = 1$) for $R/h = 20$

	L/mR		
	0.1	4	100
Dimensionless frequency [18]	10.4670	0.257011	0.000665031
Error in percent			
Straight waveguide, 40 deep shell elements	1.02	−0.02	−0.02
Straight waveguide, 20 solid elements 1 layer	4.15	b	b
Straight waveguide, 60 solid elements 3 layers	2.02	b	b
Straight waveguide, 120 solid elements 3 layers	2.02	b	b
Curved waveguide, 40 deep shell elements	1.02	−0.02	−0.02
Curved waveguide, 60 solid elements 3 layers	2.02	b	0.01

Values are the error compared to Leissa [18] in percent. b indicates differences smaller than 0.01 percent.

Table 3
Modes of order 4 for $R/h = 20$

	L/mR		
	0.1	4	100
Dimensionless frequency [18]	10.5898	0.2191	0.2087
Error in percent			
Straight waveguide, 40 deep shell elements	1.00	−0.08	−0.06
Straight waveguide, 20 solid elements 1 layer	4.18	17.27	19.09
Straight waveguide, 60 solid elements 3 layers	2.04	17.09	18.89
Straight waveguide, 120 solid elements 3 layers	2.02	1.38	1.54
Curved waveguide, 40 deep shell elements	1.01	−0.10	−0.10
Curved waveguide, 60 solid elements 3 layers	2.02	b	0.02

Values are the error compared to Leissa [18] in percent. b indicates differences smaller than 0.01 percent.

Solid elements are not used in the thin-walled case because the elements aspect ratio would be very small unless an unreasonable number of elements are used.

Tables 4–6, presents calculated results for $R/h = 500$. The results are in very good agreement with Leissa.

Table 4
Zero-order mode ($n = 0$) for $R/h = 500$

	L/mR		
	0.1	4	100
Dimensionless frequency [18]	11.11103	0.464648	0.0185859
Error in percent			
Straight waveguide, 80 deep shell elements	−0.02	b	b
Curved waveguide, 40 deep shell elements	−0.02	b	b

Values are the error compared to Leissa [18] in percent. b indicates differences smaller than 0.01 percent.

Table 5
Bending mode ($n = 1$) for $R/h = 500$

	L/mR		
	0.1	4	100
Dimensionless frequency [18]	1.11049	0.256883	0.000664824*
Error in percent			
Straight waveguide, 80 deep shell elements	−0.02	b	b
Curved waveguide, 40 deep shell elements	−0.02	b	b

Values are the error compared to Leissa [18] in percent. b indicates differences smaller than 0.01 percent. *Corrected value.

Table 6
Fourth-order mode for $R/h = 500$

	L/mR		
	0.1	4	100
Dimensionless frequency [18]	1.10276	0.0353927	0.00840299
Error in percent			
Straight waveguide, 80 deep shell elements	−0.03	b	b
Curved waveguide, 40 deep shell elements	−0.02	b	b

Values are the error compared to Leissa [18] in percent. b indicates differences smaller than 0.01 percent.

In conclusion, a circular finite length cylinder has been considered. All four derived elements can model the vibration field and the calculated eigenfrequencies are compared with results by Leissa [18]. The results are in general in good agreement with Leissa. However, when the straight waveguide with deep shell elements are used a shear and membrane locking problem can appear for which the remedy is reduced integration. Also, some caution is advised when the cylinder becomes very thin. This is not a problem inherit of the waveguide FE code, but has to do with the fact that modes up to the order of $n = 25$ are located at lower frequencies than the modes of interest for some L/mR ratios. This means that many elements are needed to get accurate results even though the sought modes are of relatively low angular order.

7. Conclusions

This article presents a waveguide finite element formulation for the analysis of wave motion in structures that have constant curvature along one direction. Element formulations for isoparametric solid elements and deep shell elements are originally presented for curved waveguides, as well as for straight waveguides. The

elements can be put into an assembly and together with the thin-walled conical shell and the fluid and fluid–structure coupling elements presented by Nilsson [5], the wave motion of a large class of curved structures can be modelled. The waveguide FE formulation is based on a modified version of Hamilton's principle for general viscoelastic material. This principle is formulated in terms of a strain potential, a kinetic potential and a load potential. These potentials are symmetric bilinear functionals of the displacement in the system of interest and in, a mathematically designed, adjoint system. Similar formulations are found in Refs. [10,11,16,19–21] while the demonstration for general linear viscoelastic material is originally presented here.

A simple validation example for the new elements, namely a circular finite length cylinder, is considered. This structure can be modelled with all four elements and the results for eigenfrequencies are compared and a small convergence study is made. The results are generally in good agreement with the exact results in Ref. [18]. However, when the straight waveguide with deep shell elements is considered, a shear and membrane locking problem can appear for which the remedy is reduced integration. Also, some caution is advised when the cylinder wall becomes very thin, since for such cylinders the low angular order modes cannot be accurately calculated unless many of the higher order modes are resolved.

The elements for curved waveguides are in Ref. [12] used to model a car tyre where the model is validated with an experimental modal analysis as well as point and transfer mobility measurements. The model also provides good results for the vibrations of a tyre rolling on a rough surface [13]. In future work, the rolling resistance of car tyres will be studied. This provides the motivation for the use of complex material models.

Acknowledgments

The early development of these elements was funded by the Swedish Research Council (621-2002-5661) and the European Commission (G3RD-CT-2000-00097). Many thanks to the members of the Ratin consortium and in particular to Roger Pinnington, ISVR, and Wolfgang Kropp, Chalmers, for helpful discussion. The final development of the elements were funded by the European Commission, ITARI, FP6-PL-0506437. Special thanks to Carl-Magnus Nilsson.

Appendix A. The stress–strain operator

Consider the following integral:

$$I = \int_{-\infty}^{\infty} u(t)\mathscr{D}(v(t))\,\mathrm{d}t = \int_{-\infty}^{\infty} u(t)\left(\int_{-\infty}^{t} G(t-\tau)\frac{\partial v(\tau)}{\partial \tau}\,\mathrm{d}\tau\right)\mathrm{d}t$$
$$= \int_{-\infty}^{\infty} u(t)\left(\int_{-\infty}^{\infty} G(t-\tau)\frac{\partial v(\tau)}{\partial \tau}\,\mathrm{d}\tau\right)\mathrm{d}t, \tag{A.1}$$

where it was used that $G(t)$ is zero for negative arguments, since motion is causal. The derivation of the operator $\mathscr{D}^a$ that is adjoint to $\mathscr{D}$ requires that the Fourier transforms of the functions in Eq. (A.1) exist. The Fourier transform is given by

$$\mathfrak{F}(u(t)) \equiv \tilde{u}(\omega) = \frac{1}{\sqrt{2\pi}}\int_{-\infty}^{\infty} u(t)\mathrm{e}^{\mathrm{i}\omega t}\,\mathrm{d}t. \tag{A.2}$$

Parseval's formula [19, p. 458] is applied on the two terms in the integrand of equation (A.1):

$$I = \int_{-\infty}^{\infty} \tilde{u}^*(\omega)\mathfrak{F}\left(\int_{-\infty}^{\infty} G(t-\tau)\frac{\partial v(\tau)}{\partial \tau}\,\mathrm{d}\tau\right)\mathrm{d}\omega$$
$$= \int_{-\infty}^{\infty} \tilde{u}^*(\omega)(\sqrt{2\pi}\tilde{G}(\omega)(-\mathrm{i}\omega\tilde{v}(\omega)))\,\mathrm{d}\omega, \tag{A.3}$$

where $\tilde{u}^*$ is the complex conjugate of $\tilde{u}$ and the Faltung theorem was applied in the second step [19, p. 465].

The integral I is real, so its value is not altered if the complex conjugate of the integrand is considered, and the terms are reordered,

$$I = \int_{-\infty}^{\infty} \tilde{v}^*(\omega)(\sqrt{2\pi}\tilde{G}^*(\omega)(\mathrm{i}\omega\tilde{u}(\omega)))\,\mathrm{d}\omega. \tag{A.4}$$

$\tilde{G}(\omega)$ is the Fourier transform of the real valued function $G(t)$, it follows that $\tilde{G}^*(\omega)$ is the Fourier transform of $G(-t)$. Upon this basis, it is possible to invert the operations that transformed Eq. (A.1) to (A.3):

$$\begin{aligned} I &= \int_{-\infty}^{\infty} -\tilde{v}^*(\omega)(\sqrt{2\pi}\tilde{G}^*(\omega)(-\mathrm{i}\omega\tilde{u}(\omega)))\,\mathrm{d}\omega \\ &= \int_{-\infty}^{\infty} v(t)\left(-\int_{-\infty}^{\infty} G(\tau - t)\frac{\partial u(\tau)}{\partial \tau}\,\mathrm{d}\tau\right)\mathrm{d}t. \end{aligned} \tag{A.5}$$

From which it follows that

$$\mathscr{D}^a(u(t)) = -\int_t^{\infty} G(\tau - t)\frac{\partial u(\tau)}{\partial \tau}\,\mathrm{d}\tau. \tag{A.6}$$

Appendix B. Demonstration of the modified Hamilton's principle

The main body of this text uses matrix algebra notation, since this is most convenient for computer implementation. If instead tensor notation is used, principle (19) is given by

$$\begin{aligned} 0 &= \delta \int 2(\hat{U} - \hat{K} + \hat{A})\,\mathrm{d}t \\ &= \int_V \sigma_{ij}\delta\varepsilon_{ij}^A + \sigma_{ij}^A\delta\varepsilon_{ij} - \rho\frac{\partial\delta u_i^A}{\partial t}\frac{\partial u_i}{\partial t} - \rho\frac{\partial u_i^A}{\partial t}\frac{\partial\delta u_i}{\partial t}\,\mathrm{d}V\,\mathrm{d}t \\ &\quad - \int\int_V f_i\delta u_i^A + f_i\delta u_i\,\mathrm{d}V\,\mathrm{d}t - \int\int_{S_\sigma} n_j(T_{ij}\delta u_i^A + T_{ij}\delta u_i)\,\mathrm{d}S\,\mathrm{d}t \end{aligned} \tag{B.1}$$

where Eq. (15) was used. It is assumed that there are no variations at the start and end of the time interval considered.

The stress tensors are symmetric and therefore

$$\sigma_{ij}\delta\varepsilon_{ij}^A = \sigma_{ij}\frac{1}{2}\left(\frac{\partial\delta u_i^A}{\partial x_j} + \frac{\partial\delta u_j^A}{\partial x_i}\right) = \sigma_{ij}\frac{\partial\delta u_i^A}{\partial x_j}. \tag{B.2}$$

Eq. (B.2) is inserted into Eq. (B.1), Gauss' theorem is applied to the first two terms in (B.1), the next two terms are integrated by parts and the remaining terms are just reordered. Upon this basis, it follows that

$$\begin{aligned} 0 &= \delta \int 2(\hat{U} - \hat{K} + \hat{A})\,\mathrm{d}t \\ &= \int\int_V \left(-\frac{\partial\sigma_{ij}}{\partial x_j} + \rho\frac{\partial^2 u_i}{\partial t^2} - f_i\right)\delta u_i^A + \left(-\frac{\partial\sigma_{ij}^A}{\partial x_j} + \rho\frac{\partial^2 u_i^A}{\partial t^2} - f_i\right)\delta u_i\,\mathrm{d}V\,\mathrm{d}t \\ &\quad + \int\int_S n_j\sigma_{ij}\delta u_i^A + n_j\sigma_{ij}^A\delta u_i\,\mathrm{d}S\,\mathrm{d}t - \int\int_{S_\sigma} n_jT_{ij}\delta u_i^A + n_jT_{ij}\delta u_i\,\mathrm{d}S\,\mathrm{d}t, \end{aligned} \tag{B.3}$$

where $S = S_u \cup S_\sigma$ is the boundary and S_u is the part of it where displacements are prescribed. It follows from the fundamental lemma of the calculus of variations that principle (19) implies the equations of motion

$$-\frac{\partial\sigma_{ij}}{\partial x_j} + \rho\frac{\partial^2 u_i}{\partial t^2} = f_i, \quad -\frac{\partial\sigma_{ij}^A}{\partial x_j} + \rho\frac{\partial^2 u_i^A}{\partial t^2} = f_i \tag{B.4}$$

and the boundary conditions. These are natural boundary conditions on S_σ

$$n_j\sigma_{ij} = n_j T_{ij}, \quad n_j\sigma_{ij}^A = n_j T_{ij} \tag{B.5}$$

and essential boundary conditions on S_u

$$\delta u_i = 0, \quad \delta u_i^A = 0. \tag{B.6}$$

The converse theorem, that Eqs. (B.4) and (B.5) implies principle (19) will now be demonstrated.

The first equation in Eq. (B.4) is multiplied with a virtual displacement δu_i^A and integrated over the volume

$$\int_V \frac{\partial \sigma_{ij}}{\partial x_j}\delta u_i^A \,\mathrm{d}V = \int_V \rho \frac{\partial^2 u_i}{\partial t^2}\delta u_i^A \,\mathrm{d}V - \int_V f_i \delta u_i^A \,\mathrm{d}V_i. \tag{B.7}$$

The first equation of Eq. (B.5) is multiplied with a virtual displacement δu_i^A and integrated over the surface

$$\int_S n_j T_{ij}\delta u_i^A \,\mathrm{d}S = \int_S n_j \sigma_{ij}\delta u_i^A \,\mathrm{d}S. \tag{B.8}$$

Now Gauss' theorem is applied:

$$\int_S n_j\sigma_{ij}\delta u_i^A \,\mathrm{d}S = \int_V (\sigma_{ij}\delta u_i^A)_{,j} \,\mathrm{d}V = \int_V \sigma_{ij,j}\delta u_i^A + \sigma_{ij}\delta u_{i,j}^A \,\mathrm{d}V. \tag{B.9}$$

The first term on the right-hand side can be substituted by Eq. (B.7), the terms are rearranged, Eq. (B.2) is used and the result is

$$\int_V f_i \delta u_i^A \,\mathrm{d}V + \int_{S_\sigma} n_j T_{ij}\delta u_i^A \,\mathrm{d}S = \int_V \rho \frac{\partial^2 u_i}{\partial t^2}\delta u_i^A + \sigma_{ij}\delta\varepsilon_{ij}^A \,\mathrm{d}V. \tag{B.10}$$

If the same operations are performed to the second equation of Eqs. (B.4) and (B.5), but the virtual displacements are taken as δu_i a similar equation to (B.10) appears. This equation can be added to Eq. (B.10) and we get

$$\begin{aligned}\int_V f_i\delta u_i^A + f_i\delta u_i \,\mathrm{d}V + \int_{S_\sigma} n_j(T_{ij}\delta u_i^A + T_{ij}\delta u_i)\,\mathrm{d}S \\ = \int_V \rho\frac{\partial^2 u_i}{\partial t^2}\delta u_i^A + \rho\frac{\partial^2 u_i^A}{\partial t^2}\delta u_i + \sigma_{ij}\delta\varepsilon_{ij}^A + \sigma_{ij}^A\delta\varepsilon_{ij}\,\mathrm{d}V.\end{aligned} \tag{B.11}$$

The next step is to integrate this expression over time. It is assumed that the variation is zero at the start and end points of the time intervall. The two first terms of the second row of Eq. (B.11) are integrated by parts and the terms are rearranged

$$\begin{aligned}0 = &\int\int_V \sigma_{ij}\delta\varepsilon_{ij}^A + \sigma_{ij}^A\delta\varepsilon_{ij} - \rho\frac{\partial\delta u_i^A}{\partial t}\frac{\partial u_i}{\partial t} - \rho\frac{\partial u_i^A}{\partial t}\frac{\partial\delta u_i}{\partial t}\,\mathrm{d}V\,\mathrm{d}t \\ &- \int\int_V f_i\delta u_i^A + f_i\delta u_i\,\mathrm{d}V\,\mathrm{d}t - \int\int_{S_\sigma} n_j(T_{ij}\delta u_i^A + T_{ij}\delta u_i)\,\mathrm{d}S\,\mathrm{d}t \\ = &\,\delta\int 2(\hat{U} - \hat{K} + \hat{A})\,\mathrm{d}t\end{aligned} \tag{B.12}$$

which is the principle.

Appendix C. Pre-loaded curved shell

A structure subjected to large static forces is deformed and internal stresses are induced, so that the structure is in a state of static equilibrium. Linear vibroacoustic analysis considers small vibrations about this state. Dynamic forces are then developed, which are given by the static stresses and strain that is proportional to the square of the displacement.

The shell element that is developed here considers in-plane, membrane, static pre-stress. Washizu [27, Eqs. (9.82), (9.33)] gives the following expression for the nonlinear in-plane strain:

$$e_{\xi\xi,nl} = \frac{1}{2}\sum_{p=1}^{3}(l_{p1})^2, \quad e_{\phi\phi,nl} = \frac{1}{2}\sum_{p=1}^{3}(l_{p2})^2, \quad e_{\xi\phi,nl} = \frac{1}{2}\sum_{p=1}^{3} l_{p1}l_{p2}, \tag{C.1}$$

where

$$\begin{aligned} l_{11} &= \frac{1}{A}\frac{\partial u}{\partial \xi} + \frac{w}{AB}\frac{\partial A}{\partial \phi} + \frac{v}{R_\xi}, \quad l_{12} = \frac{1}{B}\frac{\partial u}{\partial \phi} - \frac{w}{AB}\frac{\partial B}{\partial \xi}, \\ l_{21} &= \frac{1}{A}\frac{\partial w}{\partial \xi} - \frac{u}{AB}\frac{\partial A}{\partial \phi}, \quad l_{22} = \frac{1}{B}\frac{\partial w}{\partial \phi} + \frac{u}{AB}\frac{\partial B}{\partial \xi} + \frac{v}{R_\phi}, \\ l_{31} &= \frac{1}{A}\frac{\partial v}{\partial \xi} - \frac{u}{R_\xi}, \quad l_{32} = \frac{1}{B}\frac{\partial v}{\partial \phi} - \frac{w}{R_\phi}. \end{aligned} \tag{C.2}$$

It follows that the strain energy induced by the static pre-load is given by

$$E_{pp} = \int \sum_{n=0}^{1}\sum_{m=0}^{1} \frac{\partial^n \mathbf{v}^{\mathrm{H}}}{\partial \phi^n}\mathbf{P}_{nm}\frac{\partial^m \mathbf{v}}{\partial \phi^m}\,\mathrm{d}\phi, \tag{C.3}$$

where

$$\mathbf{P}_{nm} = \int_{-1}^{1}\left(N_\xi \sum_{p=1}^{3}\mathbf{l}_{p1n}^{\mathrm{T}}\mathbf{l}_{p1m} + N_\phi \sum_{p=1}^{3}\mathbf{l}_{p2n}^{\mathrm{T}}\mathbf{l}_{p2m} + \frac{N_{\xi\phi}}{2}\sum_{p=1}^{3}\mathbf{l}_{p1n}^{\mathrm{T}}\mathbf{l}_{p2m} + \mathbf{l}_{p2n}^{\mathrm{T}}\mathbf{l}_{p1m}\right)AB\,\mathrm{d}\xi, \tag{C.4}$$

$$\begin{aligned} \mathbf{l}_{110} &= \mathbf{h}'\mathbf{B}_u/A + \mathbf{h}\mathbf{B}_v/R_\xi, \\ \mathbf{l}_{210} &= \mathbf{h}'\mathbf{B}_w/A, \\ \mathbf{l}_{310} &= \mathbf{h}'\mathbf{B}_v/A - \mathbf{h}\mathbf{B}_u/R_\xi, \\ \mathbf{l}_{111} &= 0, \\ \mathbf{l}_{211} &= 0, \\ \mathbf{l}_{311} &= 0, \end{aligned} \tag{C.5}$$

$$\begin{aligned} \mathbf{l}_{120} &= -B_p\mathbf{h}\mathbf{B}_w, \\ \mathbf{l}_{220} &= B_p\mathbf{h}\mathbf{B}_u + \mathbf{h}\mathbf{B}_v/R_\phi, \\ \mathbf{l}_{320} &= -\mathbf{h}\mathbf{B}_w/R_\phi, \\ \mathbf{l}_{121} &= \mathbf{h}\mathbf{B}_u/B, \\ \mathbf{l}_{221} &= \mathbf{h}\mathbf{B}_w/B, \\ \mathbf{l}_{321} &= \mathbf{h}\mathbf{B}_v/B. \end{aligned} \tag{C.6}$$

where N_ξ, N_ϕ and $N_{\xi\phi}$ are the static forces (per unit length).

References

[1] P.E. Lagasse, Higher-order finite-element analysis of topographic guides supporting elastic surface waves, *The Journal of the Acoustical Society of America* 53 (4) (1973) 1116–1122.
[2] B. Alaami, Waves in prismatic guides of arbitrary cross section, *Journal of Applied Mechanics* December (1973) 1067–1071.
[3] S. Finnveden, Evaluation of modal density and group velocity by a finite element method, *Journal of Sound and Vibration* 273 (2004) 51–75.
[4] S. Finnveden, Exact spectral finite element analysis of stationary vibrations in a rail way car structure, *Acta Acustica* 2 (1994) 461–482.
[5] C.-M. Nilsson, Waveguide Finite Elements Applied on a Car Tyre, PhD Thesis, MWL, KTH, TRITA-AVE, 2004, p. 21.
[6] V. Damljanovic, R.L. Weaver, Propagating and evanescent elastic waves in cylindrical waveguides of arbitrary cross section, *Journal of the Acoustical Society of America* 115 (2004) 1572–1581.

[7] P.J. Shorter, Wave propagation and damping in linear viscoelastic laminates, *Journal of the Acoustical Society of America* 115 (2004) 1917–1925.
[8] I. Bartoli, A. Marzani, F. Lanza diScalea, E. Viola, Modeling wave propagation in damped waveguides of arbitrary cross-section, *Journal of Sound and Vibration* 295 (2006) 685–707.
[9] U. Orrenius, Y.-Y. Pang, B. Stegeman, S. Finnveden, Acoustic modelling of extruded profiles for railway cars, *Proceedings of November Saint Raphael*, 2005.
[10] C.-M. Nilsson, S. Finnveden, Input power to waveguides calculated by a finite element method, *Journal of Sound and Vibration* 305 (2007) 641–658.
[11] F. Birgersson, S. Finnveden, C.-M. Nilsson, A spectral super element for modelling of plate vibration: part 1, general theory, *Journal of Sound and Vibration* 287 (2005) 297–314.
[12] M. Fraggstedt, Power Dissipation in Car Tyres, Licentiate Thesis, MWL, KTH, TRITA-AVE, 2006, p. 26, ⟨http://www.ave.kth.se/publications/mwl/downloads/TRITA-AVE_2006-26.pdf⟩.
[13] S. Finnveden, C.-M. Nilsson, M. Fraggstedt, Waveguide FEA of the vibration of rolling car tyres, *Proceedings of November*, *Saint Raphael*, 2005.
[14] O.C. Zienkiewicz, R.L. Taylor, *The Finite Element Method*, fourth ed., McGraw-Hill, New York, 1989.
[15] D.S. Burnett, *Finite Element Analysis, from Concepts to Applications*, Addison-Wesley, Reading, MA, 1987.
[16] S. Finnveden, Spectral finite element analysis of the vibration of straight fluid-filled pipes with flanges, *Journal of Sound and Vibration* 199 (1997) 125–154.
[17] Y.C. Fung, P. Tong, *Classical and Computational Solid Mechanics*, World Scientific Publishing, Singapore, 2001.
[18] A.W. Leissa, *Vibrations of Shells (NASA-SP-288)*, US Government Printing Office, Washington, DC, 1973.
[19] P.M. Morse, H. Feshbach, *Methods of Theoretical Physics*, McGraw-Hill, New York, 1953.
[20] G.M.L. Gladwell, A variational formulation for damped acusto-structural problems, *Journal of Sound and Vibration* 4 (1966) 172–186.
[21] P.M. Morse, U.K. Ingard, *Theoretical Acoustics*, Princeton University Press, Princeton, NJ, 1968.
[22] R.L. Bagley, P.J. Torvik, Fractional calculus—a different approach to the analysis of viscoelastic structures, *AIAA Journal* 21 (1983) 741–748.
[23] T. Hayashi, K. Kawashima, Z. Sun, J.L. Rose, Guided wave propagation mechanics across a pipe elbow, *Journal of Pressure Vessel Technology* 127 (2005) 322–327.
[24] A. Demma, P. Cawley, M. Lowe, B. Pavlakovic, The effects of bends on the propagation of guided waves, *Journal of Pressure Vessel Technology* 127 (2005) 328–335.
[25] K. Dovstam, Augmented Hooke's law in frequency domain. A three dimensional material damping formulation, *International Journal of Solids and Structures* 32 (1995) 2835–2853.
[26] K. Dovstam, Augmented Hooke's law based on alternative stress relaxation models, *Computational Mechanics* 26 (2000) 90–103.
[27] K. Washizu, *Variational Methods in Elasticity and Plasticity*, Pergamon Press, Oxford, 1975.
[28] R. Cook, *Concepts and Applications of Finite Element Analysis*, fourth ed., Wiley, New York, 2002.